Revision 3

Influence of organic matter on smectite illitization: a comparison between red and dark mudstones from the Dongying Depression, China

Yingli Li[1], Jingong Cai[1,*], Mingshui Song[2], Junfeng Ji[3], Yujin Bao[2]

[1] State Key Laboratory of Marine Geology, Tongji University, Shanghai 200092, China

[2] Geological Scientific Research Institute, Shengli Oil Field Company, Sinopec, Dongying 257015, China

[3] Department of Earth Sciences, Nanjing University, Nanjing 210093, China

ABSTRACT

Interactions between organic matter (OM) and clay minerals have received considerable attention in previous studies. The influence of OM on smectite illitization has been analyzed primarily in simulation experiments rather than in diagenetic studies. The present study explores the influence of OM on smectite illitization during diagenesis. Thirty red and dark mudstone samples from the Dongying Depression were analyzed. X-ray diffraction (XRD) analyses revealed that the illite percentages in mixed-layer illite-smectite (I-S) of both types of samples were dispersive above 3100 m and more convergent below this depth. The stacking mode of I-S in dark mudstones above 3100 m remained primarily at R0-R0.5 ordering with the average number of layers (N_{ave})

* Corresponding author. Tel.: +86 21 6598 8829.

E-mail address: jgcai@tongji.edu.cn.

Mail address: Tongji University, School of Ocean and Earth Science, Room 613, Siping Road 1239, 200092, Shanghai, China

dispersively distributed between 2 and 4.5. In red mudstones, the I-S changed from the R0 to R0.5 mode with the N_{ave} increasing from 2 to 5. Over this range, the smectite illitization in dark mudstones was slower than that in red mudstones. Below 3100 m, the I-S stacking mode of dark mudstones changed from R0.5 to R3 ordering with the N_{ave} increasing sharply from 4 to 8. In red mudstones, the I-S displayed R1.5 and R3 ordering with the N_{ave} varying between 4.5 and 6.5. Over this range, the smectite illitization in dark mudstones accelerated rapidly, whereas the process in red mudstones was retarded. Additionally, the red mudstone samples contained little OM, whereas the dark mudstone samples contained abundant total organic carbon (0.17-4.43%). Thermo-XRD, near-infrared (NIR) as well as mid-infrared (MIR) spectroscopy analyses suggested that the OM in dark mudstones exhibited a significant transition at 3100 m, coincident with the illitization change. Above 3100 m, the smectite illitization in dark mudstones was delayed due to the OM pillar effect in the interlayer spaces of smectite. Below 3100 m, the interlayer OM became varied and desorbed, discharging organic acid. This led to the dissolution of smectite structural layers. Consequently, illitization in the dark mudstone was accelerated. This study revealed that the existence and occurrence of OM could influence the smectite illitization in diagenesis. Further study on the interactions between OM and clay minerals is needed to facilitate our understanding on the mechanism of smectite illitization as well as its geological applications.

Key Words: Smectite illitization, dark mudstone, red mudstone, organic matter, Dongying Depression, reaction mechanisms

INTRODUCTION

Mudstones, particularly argillaceous source rocks, contain various levels of

inorganic matter, pore water, and organic matter (OM, Tissot and Welte, 1984; Tyson, 1993; Li and David, 2005; Pacton et al., 2011). As the two most important components in mudstones, the interactions between OM and clays have been frequently discussed (Barker, 1980; Ganor et al., 2009; Ugochukwu et al., 2013). Several studies suggested that mudstone smectite illitization can affect the occurrence and evolution of OM (Burst, 1969; Bruce, 1984). However, the counter effects of OM on smectite illitization require further investigation.

The conversion of smectite to illite is a common geologic phenomenon (Pollard, 1971; Ahn and Peacor, 1986; Altaner and Ylagan, 1997; Baronnet, 1997; Putnis, 2002; Cuadros, 2012). Various mechanisms of smectite illitization were proposed, including the broadly accepted concepts of solid-state transformation (Hower et al., 1976; Bethke and Altaner, 1986; Drits et al., 1997; Cuadros and Altaner, 1998; Olives et al., 2000) and dissolution-recrystallization (Boles and Franks, 1979; Nadeau et al., 1985; Eberl and Srodon, 1988; Whitney and Velde, 1993; Mosser-Ruck et al., 1999; Mosser-Ruck et al., 2001; Lanson et al., 2009; Bobos and Eberl, 2013). The solid-state transformation model emphasizes gradual changes in the chemical components of phyllosilicates. In contrast, the dissolution-recrystallization model emphasizes the mutation and dissolution of the smectite structural layer. These processes are assumed to occur in the water-rock environment. In all models, researchers emphasized the importance of such parameters as the temperature (Perry and Hower, 1972; Cuadros and Linares, 1996), time (Eberl and Hower, 1976; Pytte and Reynolds, 1989), cation levels (e.g., K+, Roberson and Lahann, 1981; Huang et al., 1993; Mosser-Ruck et al., 2001), and the water/rock ratio (Howard and Roy, 1985; Whitney, 1990), which appear to affect smectite illitization. In most cases,

the temperature was assumed to be a primary factor. For this reason, the proportion of illite or smectite in mixed-layer illite-smectite (I-S) is often used as an effective geothermometer to investigate basin evolution (Pollastro, 1993; Pevear, 1999; Środoń, 1999; Środoń et al., 2009; Bourdelle et al., 2013). Laboratory studies demonstrated that certain organic acids, such as oxalate (Schumann et al., 2013), acetate (Small, 1994), and ethylenediamine tetraacetic acid (EDTA, Golubev et al., 2006), can accelerate smectite illitization or crystallization. Because organic acids provide K and Al to pore fluids by dissolving the detrital smectite, K-feldspar, and muscovite, and alter the pH during their generation and decomposition, they are able to partially control the smectite illitization (Eberl et al., 1993).

Microorganisms have been reported to affect the process (Kim et al., 2004; Zhang et al., 2007a; Dong et al., 2009; Kim, 2012; Pentráková et al., 2013; Liu et al., 2014). OM in the smectite interlayer, such as cysteine and toluene, may promote or inhibit bacterial activities that affect the reduction of structural Fe (III) in smectite (Zhang et al., 2007b; Yu et al., 2012). In this case, OM has an indirect effect on smectite illitization. In general, most of this knowledge was obtained from simulation experiments. Similar studies involving diagenesis, however, are rare.

In diagenesis, OM in mudstone can be present in diverse forms, e.g., adsorbed as organic ions and molecules in pore spaces, on the external surfaces of clay crystals, or in the interlayer spaces (Garfinkel-Shweky and Yariv, 1997; Kennedy et al., 2002; Yariv and Cross, 2002; Yariv and Lapides, 2005; Naranjo et al., 2013). Because smectite has high expansibility, large internal and external specific surface areas, and high cation exchange capacity, it can adsorb certain amounts of OM within the interlayer space, and

then form clay-organic complexes (Guan and Xu, 1998; Kennedy et al., 2002; Cai et al., 2007). Usually, the adsorbed OM is transformed and desorbed during burial, generating oil, gas, and organic acid (Tissot and Welte, 1984; Barth et al., 1988; Andresen et al., 1993; Barth and Bjørlykke, 1993; Lewan and Fisher, 1994; Speight, 1999; Dias et al., 2002; Clausen et al., 2013). The transformation can affect pore fluid properties and thereby the interactions between the pore fluid and minerals. For these reasons, the role of OM in mudstone diagenesis should not be ignored. Consequently, two sequences of mudstone rocks representing water-rock-OM and water-rock systems were collected in this study to assess the effects of OM on smectite illitization during diagenesis.

MATERIALS AND METHODS

Geologic setting

The Dongying Depression, with an area of 5850 km^2, is located in the southeastern Bohai Bay Basin (Figure 1). This depression is one of the most oil-rich areas in eastern China and developed as a typical fault-depression basin during the Late Jurassic to the early Cenozoic. The Dongying Depression is bounded by the Chenjiazhuang Uplift on the north, the Qingtuozi and Guangrao Uplifts on the east, the Luxi Uplift on the south, and the Qingcheng-Linjia-Binxian Uplifts on the west (Figure 1). The Cenozoic deposits in the study area consist of continental siliciclastic rocks of the Kongdian, Shahejie, Dongying, Guantao, Minghuazhen, and Pingyuan formations, with a total thickness of 1600-5000 m. And detailed descriptions of the stratigraphy have been presented by many authors such as Feng et al. (2013) and Lei et al. (2014). In this study, thirty samples were collected from the strata with two types of comparative lithologies. Of these, 19 dark mudstone samples were collected from the Paleogene Shahejie Formation at depths of

2245-3492 m (Table 1). The depositional environment transitioned from a salt lake to a deltaic lake. The other 11 samples were red mudstones collected from the Paleogene Kongdian Formation, the Neocene Guantao Formation, and the Minghuazhen Formation at depths of 995-5271 m (Table 1). The strata primarily developed in the depositional environments of a fluvial salt lake, braided stream, and floodplain, respectively. Due to limitations of the core records, the depth ranges and sample horizons of two mudstones did not exactly match.

Insert Figure 1 here

Insert Table 1 here

Materials

The <2-μm clay fractions were prepared for analyses. To assess the OM impact on smectite illitization, no chemical treatment or cation exchange was performed during the preprocessing to avoid any removal of carbonates, (hydr)oxides, silica, and organic materials and thus any alteration of the original composition of the OM and clay minerals. The rocks were first ground into powder using a jaw crusher and a hammer mill. The samples were then placed in an ultrasonic tank at a frequency of 40 kHz and a power of 800 W for 3 hours to create a dispersed suspension. A suspension containing the <2-μm clay fraction was obtained from the suspension in accordance with Stokes' Law. These fractions were concentrated via sedimentation by centrifugation at a rate of 7200 rpm and finally dried at 40°C.

X-ray diffraction analysis

A total of 60 mg of the <2-μm clay fractions was mixed with 5 ml of deionized water and then deposited on a 25×50-mm slide glass to obtain an oriented slide (4.9 mg

134 cm^{-2}). Approximately 200 mg of the bulk samples was packed into a 20×18-mm frame by
135 side loading (Moore and Reynolds, 1997) to create a random preparation.

136 The XRD analyses were performed using a Rigaku D/max-IIIa diffractometer at 20
137 mA and 40 kV with a curved graphite monochromator. The CuKα radiation was set at
138 1.540596 Å. The scattering slit was 1° with a receiving slit of 0.3 mm. Each oriented
139 slide was scanned from 3 to 30 °2θ at 2 °2θ min^{-1} with a step width of 0.02 °2θ, and the
140 random slides were scanned from 3 to 40 °2θ at 2 °2θ min^{-1} with a step width of 0.02 °2θ.

141 Clay composition analyses were completed using the oriented slides with multiple
142 treatments: air-drying, ethylene glycol saturation, and heating (550°C). To examine the
143 variations in the interlayer spaces in smectite or I-S, thermo-XRD analyses were used.
144 Previous thermo-XRD analyses of samples of soil (Theng et al., 1986) and argillaceous
145 source rocks (Cai et al., 2007) suggested that water adsorbed in the interlamellar space of
146 clay minerals is readily removable through heating to 250°C whereas the interlayer OM
147 is more stable. The relevant basal spacing of organo-clay complexes did not attain a
148 width of 10 Å until the temperature increased to 550°C. The temperatures of 250°C and
149 550°C are therefore taken as two significant points in thermo-XRD analysis at which the
150 interlayer OM can be recognized based on their stability (Nemecz, 1981). For this reason,
151 the oriented slides received three different treatments: air drying, heating to 250°C, and
152 heating to 550°C to detect the change of the interlayer spaces in smectite or I-S.

153 The clay minerals were identified based on the position of the (001) series of basal
154 reflections in the diagrams of the air-dried, ethylene glycol-saturated, and heated (550°C)
155 XRD samples. Partial quantification was performed by calculating the integrated peak
156 areas of the mineral phases multiplied by in-house calibrated and/or published weighting

157 factors. The integrated area of the 7-Å (chlorite 002/kaolinite 001) peak in the curve from
158 the ethylene glycol-treated sample was used to quantify the amounts of chlorite and
159 kaolinite. The relative proportions of these two minerals were based on the peak heights
160 of kaolinite 002 (3.58 Å) and chlorite 004 (3.52 Å) on the glycolated curve. The
161 quantities of smectite, I-S, and illite were based on the integrated area of the 10-Å peak
162 on the 550°C heated curve. The quantity of smectite was based on the integrated area of
163 the 17-Å peak with ethylene glycol treatment, whereas that of the illite was based on the
164 integrated area of the 10-Å peak. The quantity of I-S was based on the remaining fraction,
165 i.e., excluding the kaolinite, chlorite, illite and smectite. Weighting factors of the
166 chlorite/kaolinite, smectite, and illite were 2/3, 1/4, and 1, respectively. Replicate
167 analyses of a few selected samples gave a relative precision of ±2%.

168 Bulk mineralogy analyses were performed on the random slides. The quantity of
169 each mineral was based on the integrated peak area of respective mineral phases.

170 The stacking mode (R, Reichweite ordering parameter), percentage of illite in the
171 I-S (I%), range of number of layers (N) and average number of layers (N_{ave}) in the
172 stacking sequence of the I-S were determined using the method of Moore and Reynolds
173 (1997) and the computer program NEWMOD 2.0 (Reynolds, 1985). The precision of the
174 I% determination was ±5%.

175 **TOC analysis**

176 The total organic carbon (TOC) content was analyzed using a Leco CS-444
177 instrument on bulk rocks with an oxygen pressure of 0.17 MPa, a combustion pressure of
178 0.055 MPa, and an accuracy of <0.5%. Inorganic carbon was removed with diluted
179 hydrochloric acid (5%).

Fourier transform infrared (FT-IR) spectroscopy

Infrared (IR) spectra in the middle infrared (MIR, 4000-400 cm^{-1}) region were obtained using a Nicolet 6700 spectrometer equipped with a diffuse reflectance accessory by co-addition of 128 scans at a resolution of 4 cm^{-1} and a mirror velocity of 0.6329 cm s^{-1}. To obtain the spectra a DTGS detector and a KBr beam splitter were used. The <2-μm fractions were manually ground in an agate mortar for 15 minutes. Subsequently, the powders were heated at 105°C for 24 h and were then stored in a desiccator with solid silica gel at room temperature. Approximately 200 mg of the thermally treated powder from each sample was prepared for the analyses. Spectroscopy-grade KBr was selected for the background spectrum. Smoothing and normalization of the spectra were performed using the OMNIC 8 software package (Nicolet Instruments Corporation).

IR spectra in the near infrared (NIR, 8000-4000 cm^{-1}) region were obtained using a Perkin-Elmer Lambda 6 spectrophotometer with a diffuse reflectance attachment. Sample preparation and analysis followed the procedures described in Balsam and Deaton (1991) and Pentrák et al. (2012). The <2-μm fractions were made in to a slurry on a glass microslide with distilled water, smoothed, dried slowly at low temperature (<40°C) and heated at 105°C for 24 h and then cooled to room temperature for 2 h in a desiccator with solid silica gel. Spectra manipulations were performed using the OMNIC 8 software package. The second-order derivative using Norris derivative filter (with default OMNIC parameters) was employed to analyze the NIR bands.

RESULTS

XRD analysis

XRD analysis demonstrated that both the red and dark mudstones were composed of clay minerals, debris minerals (e.g., quartz and feldspar), and carbonate minerals (e.g., calcite and dolomite). In the dark mudstone, clay minerals accounted for 13-53% of the total composition (Table 1). The proportions of clay and quartz decreased with depth, and the calcite content increased significantly. In the red mudstone, clay minerals accounted for 32-74% of the total composition (Table 1). The amounts of clay, quartz and carbonate minerals varied little with depth. In addition, pyrite was found in some dark mudstone samples while it was absent in red mudstone samples.

XRD characterization of samples (Table 1, Figure 2) further indicated that illite (average of 38% and 46% in red and dark samples, respectively) and I-S (including smectite; average of 43% and 41% in red and dark samples, respectively) were the primary clay minerals in all the samples, with trace amounts of kaolinite (average of 10% and 9% in red and dark samples, respectively) and chlorite (average of 9% and 4% in red and dark samples, respectively). The clay mineral evolution in the mudstones displayed a bimodal feature (Figure 2). Above 3100 m, the red mudstone contained a greater amount of illite (2-60%) as well as less I-S and smectite (30-89%) than the dark mudstone (11-32% and 51-75% respectively, Figures 2a, b). The kaolinite proportions in the two types of mudstone were slightly greater than that of chlorite (Figures 2c, d). Below 3100 m, the illite proportion in the red mudstones reached approximately 70%, whereas the I-S proportion decreased to approximately 10% (Figures 2a, b). In the dark mudstones, the illite proportion increased significantly to 91%, and the I-S proportion rapidly decreased

223 to 9% (Figures 2a, b). Simultaneously, the amount of chlorite in the red mudstone
224 increased sharply to 16%, while it remained stable (Figure 2d) in the dark mudstone.

225 Insert Figure 2 here

226 The I% of dark mudstone samples ranged from 51% to 80% above 3100 m, and that
227 of red mudstone samples varied from 30% to 83%, all showed a distinct variation during
228 this interval (Table1, Figure 2e). I% of the dark mudstone samples was ubiquitously less
229 than that of the red mudstone samples at the same depth (Figure 2e). Below 3100 m, I%
230 of the dark mudstone samples increased gradually from 83% to 90%, and that of the red
231 mudstone samples ranged from 90% to 92%. Their differences generally decreased with
232 depth. The maximum difference of I% between red and dark mudstone samples was
233 approximately 35% at 2200 m but decreased to 0% at 3500 m.

234 With a maximum value of 6.5, the N_{ave} of the red mudstones increased slowly with
235 depth from 1000 m to 5500 m (Table1, Figure 2f). Above 3100 m, the N_{ave} of the dark
236 mudstones were dispersive and ranged from 2 to 4.5 (Table1, Figure 2f), which was
237 generally smaller than that of the red mudstone from the same horizon (Figure 2f). Below
238 3100 m (Figure 2f), the N_{ave} of the dark mudstone samples increased rapidly from 4 to 8
239 within 400 m (depth 3100 m to 3500 m), which indicates an increase in crystal growth. In
240 contrast, that of the red mudstone generally remained at approximately 5.5 within 2200 m
241 (depth 3100 m to 5300 m).

242 In all the samples, the I-S stacking mode changed from R0 to R0.5, R1.5 and R3
243 ordering (Table 1, Figures 3, 4) with depth, indicating a transformation of smectite to
244 illite. The red mudstone samples display an R0 mode of the I-S above 2200 m. At greater
245 depths, the mode gradually transitioned to types R0.5, R1.5, and R3.0 (Figures 3a, 4).

The dark mudstone samples display R0 and R0.5 modes above 3100 m (Figures 3b, 4), which were generally lower than those of the red mudstone in the same horizon. In the depth range of 3100-3500 m, the stacking mode of the dark mudstone samples changed sharply from R0.5 to R1 and R3. Below 4000 m, the red mudstones display R1.5 and R3 modes and did not reach the R3 mode until a depth of 4500 m (Figure 4).

Insert Figure 3 here

Insert Figure 4 here

TOC characteristics

The TOC analyses (Table 1, Figure 5) revealed that the red mudstone samples contained little OM (TOC concentrations of 0.01-0.14%), whereas the dark mudstone was rich in OM (TOC concentrations of 0.17-4.43%). In addition, the TOC distribution displayed a distinct bimodal variation in the dark mudstone with depth (Table 1, Figure 5b). Above depths of 3100 m, the TOC content of the dark mudstone ranged from 0.39 to 3.28% (1.57% on average), whereas it generally ranged from 0.17 to 4.43% below 3100 m (2.17% on average).

Insert Figure 5 here

Thermo XRD analysis

Thermo-XRD analyses was used to detect the penetration of OM into the interlayer spaces of smectite (Nemecz, 1981; Yariv and Lapides, 2005). Below 1500 m, all the I-S basal spacing (001) of the red mudstone remained at 1.0 nm (Figure 6a) at 250°C. The I-S basal spacing (001) exceeded 1.0 nm to more than 1.36 nm (Figure 6a) at 250°C above 1500 m. The XRD patterns from the dark mudstone between 2200 m and 3100 m showed that the d_{001} diffraction ranged from 1.10 nm to 1.39 nm at 250°C and stayed around 1.0

nm at 550°C (Figure 6b). Certain uniform gaps (Figures 6b, 7b) between the 250°C and 550°C curves occurred to the left of the I-S d_{001} diffraction. Below 3100 m, the difference in I-S d_{001} position between XRD patterns at 250°C and 550°C was unconspicuous (Figures 6b, 7b).

Insert Figure 6 here

Insert Figure 7 here

Infrared analysis

The MIR spectroscopic analysis focused on the stretching (3100-2700 cm^{-1}) region of CH groups (Figure 8). In spectra of the dark mudstone samples, bands near 2926 cm^{-1} and 2854 cm^{-1} (Figure 8b) were attributed to the antisymmetric ($\nu_{as}(CH_2)$) and symmetric ($\nu_s(CH_2)$) stretching modes of aliphatic CH_2 (Alstadt et al., 2012), thus marking the most prominent organic functional group in the MIR spectra. The band intensity of the CH_2 stretching vibration increased with depth. The aromatic CH_2 stretching vibration, however, was relatively weak. This vibration was observed at approximately 3050 cm^{-1} (Figure 8b). No clear CH_3 stretching band was observed in the spectrum. The red mudstone spectra displayed no CH stretching modes, and the vibrations in the 3000-2900-cm^{-1} region were attributed to the distortions of CO_3^{2-} antisymmetric stretching vibrations (Nguyen et al., 1991; Ge et al., 2009, Figure 8a).

Insert Figure 8 here

The spectra in the NIR region of red and dark mudstone samples displayed an intensive band near 5250 cm^{-1} (Figure 9). This corresponded to the combination of the stretching and bending vibrations of $(\nu+\delta)H_2O$ bound in montmorillonite (Pentrák et al., 2012; Brtáňová et al., 2014). The complex band near 7080 cm^{-1} (Figure 9) corresponded

to the overlapping by the first overtone of stretching vibrations of structural OH groups in montmorillonite and that of H_2O molecules (Madejová et al., 2009). The overtone and combination bands of CH stretching vibrations were however not so clearly resolved as did in the MIR spectra. The intensity of the $(\nu+\delta)H_2O$ band at 5250 cm^{-1} decreased with depth. The band at 7080 cm^{-1} almost disappeared in red and dark mudstone samples below 3100 m (Figure 9).

Insert Figure 9 here

DISCUSSION

Characteristics of smectite illitization

Defined by the depth of 3100 m, the analyses of clay minerals in red and dark mudstones revealed a bimodal feature (Figures 2, 3, 4) which was defined a in aspects of their mineral evolution, I-S stacking modes, crystallinity characteristics as well as I% differences. Above 3100 m, the illite content in red mudstones was higher and the I-S content lower than that in dark mudstones (Figures 2a, b). The difference of I% between the two types of rocks was dispersive during this depth range (Figure 2e). And I-S in the dark mudstones displayed R0 and R0.5 modes which were generally lower than those of the red mudstones at the same horizon (Figures 3, 4). In addition, the N_{ave} of dark mudstones was smaller than that of the red mudstones from the same horizon (Figure 2f). The characteristics indicated that the I-S crystallinity of red mudstones was significantly better than that of dark mudstones. In a word, the smectite illitization in red mudstones was faster than that in dark mudstones. Below 3100 m, changes in the illite and I-S proportions of red mudstones slowed (Figures 2a, b) while that of dark mudstones varied significantly. And the differences of I% values were more convergent below this depth

(Figure 2e). These characteristics indicated that the smectite illitization in dark mudstones accelerated and approached its completion in this range. Meanwhile, the radical change of stacking mode in the dark mudstones (Figures 3b, 4) between 3100-3500 m indicates that the stacking order of the I-S improved and the illitization increased. The R1.5 and R3 modes of red mudstones below 4000 m indicated a much weaker illitization (Figure 4). The rapid rise of the N_{ave} of dark mudstones (Figure 2f) indicated an increase in crystal growth. As that of the red mudstone generally remained unchanged within 2200 m (depth 3100 m to 5300 m), it was consequently inferred that the I-S of dark mudstones got a high crystallinity at relatively shallower depth. This implies that the I-S of the dark mudstone developed faster than that of the red mudstone below 3100 m. Generally speaking, the characteristics of clay minerals displayed various differences in the smectite illitization of red and dark mudstones from the same basin, and the rate of illitization in the mudstones was inconsistent at 3100 m.

Characteristics of OM

The basic difference between red and dark mudstones is that the red mudstones contain little OM whereas the dark mudstones own abundant OM (Figure 5) with distinct occurrences above/ below 3100 m. In red mudstones below 1500 m, a lack of OM or any other filling material in the interlayer spaces of the smectite or I-S was indicated by the 1.0 nm of I-S d_{001} diffraction at 250°C (Figure 6a). Above 1500 m, the enlarged I-S basal spacing (001) (Figure 6a) at 250°C suggested the presence of an unknown material in the interlayer spaces. Considering the low proportion of TOC, the filling materials should not be OM. In dark mudstones above 3100 m, the lag between the d_{001} diffraction at 250°C and 550°C (Figure 7b) confirmed the presence of OM in the interlayer spaces of smectite

or I-S (Theng et al., 1986; Yariv and Lapides, 2005; Cai et al., 2007). Uniform gaps (Figures 6b, 7b) between the 250°C and 550°C curves indicated that the interlayer OM in dark mudstones was stable over this range. As the difference in I-S d_{001} position between XRD patterns at 250°C and 550°C became unconspicuous (Figures 6b, 7b) below 3100 m, the interlayer OM is suggested to become unstable and even absent in various horizons.

In addition, through the NIR spectra analysis, information about the interaction between OM and clay minerals in dark mudstones can be detected. Considering that the samples were heated at 105°C for 24 h, water adsorbed to interstitial pores or polar external surfaces was removed (Russell and Farmer, 1964). Thus the detected water was actually the firmly bonded interlamellar water which can be coordinated to exchangeable metallic cations to connect organic species and clay minerals in the form of hydrogen bond or protonated base (Yariv and Cross, 2002). Thus in dark mudstone samples which were rich in OM, H_2O would probably be a bridge to connect OM and clay. The obvious decrease of the intensity of the band near 5250 cm^{-1} (Figure 9b) reflected the decrease of water in the interlayer space of clay minerals and the weaken of hydrogen bond between OM and clay minerals (Madejová et al., 2009; Pentrák et al., 2012). This suggested that the amount of water-bridged interlayered OM decreased below 3100 m.

As discussed above, both the smectite illitization and the distribution of OM in the red and dark mudstones displayed clear differences. Moreover, the illitization exhibited a bimodal property in the dark mudstone coincident with the OM transition at 3100 m. Taken together, these data indicate that the presence of OM affected the smectite illitization.

Influences of the OM on smectite illitization

Because smectite and illite are 2:1 phyllosilicates (Grim, 1953; Weaver and Pollard, 1973; Bergaya et al., 2011), they differ primarily in their interlayer compositions. The interlayer spaces of smectite contain interlamellar water and cations such as Mg^{2+} and Ca^{2+}. The interlayer spaces of illite, however, contain only K^{+}. Thus, the exchange of interlayer cations is an effective means of transforming smectite to illite. Accordingly, the solid-state transformation model was proposed (Hower et al., 1976; Bethke and Altaner, 1986; Drits et al., 1997; Cuadros and Altaner, 1998; Olives et al., 2000), which proceeded progressively with depth. Above 3100 m, the gradual variation of clay mineralogy (Table 1; Figures 2, 3, 4) indicated the model performed in both of the red and dark mudstones. It should be noted that when the solid-state model was applied to the dark mudstone (Table 1; Figures 2, 3b, 4), however, it may be affected by the abundant OM in the smectite interlayer spaces. In the dark mudstone, clay minerals and OM, particularly the OM in the interlayer spaces of the smectite, bond together via ionic bonds, hydrogen bonds, and water bridge bonds (Mortland, 1970; Theng, 1974, 1979; Xiong et al., 1983; Yu et al., 2013) to form organo-clay complexes. Cai (2011) reported that the interlayer OM of organo-clay complexes may partially delay the dehydration of interlamellar water due to water “bridges” that bonded OM and smecitie. And the stability of interlayer OM was strengthened when combined to montmorillonite through exchangeable high state cations (Pusino et al., 1993). For this reason the exchange of interlayer cations was be delayed. Furthermore, the interlayer OM is extremely resistant to heat damage and organic solvent destruction (Theng et al., 1986; Schulten et al., 1996; Lu et al., 1999; Yariv and Cross, 2002; Cai et al., 2013), which strengthens its delay effect. All of these

383 effects hindered smectite illitization during diagenesis and were particularly prominent in
384 the dark mudstones above 3100 m (Figures 2, 4).

385 In MIR spectra of dark mudstone samples, the vibration peak area of aliphatic CH_2
386 in the 3000-2800-cm^{-1} stretching region has a positive correlation with the TOC content
387 with a coefficient of 0.81 (Figure 10). Therefore, information regarding to the evolution
388 of the OM can be acquired by analyzing the aliphatic OM. Moreover the peak area of the
389 CH_2 vibration first gradually increased with burial depth (Figure 11) and then increased
390 more rapidly below 3100 m, reaching a maximum at approximately 3400 m (Figures 8b,
391 11). Thus the peak area of the aliphatic CH_2 band displayed an apparent bimodal
392 variation with depth, a pattern similar to that of the TOC content variation (Figure 5b). It
393 is generally indicated that the total OM increased with depth in dark mudstones.

394 Insert Figure 10 here

395 Insert Figure 11 here

396 On the other hand, the thermo-XRD data confirmed that the interlayer OM of the I-S
397 became unstable and even absent in many layers below 3100 m (Figure 6b). The NIR
398 spectra showed that the intensity of the interlayer water band 5250 cm^{-1} decreased
399 remarkably below 3100 m (Figure 9). This further confirmed that the interlayer OM
400 combined to clays through water bridges decreased.

401 In conclusion, the total OM increased (Figures 5b, 11) whereas the interlayer OM
402 decreased below 3100 m. Hence, it is concluded that the OM, including but not limited to
403 the interlayer OM, was transferred to other places, e.g., being adsorbed as organic ions
404 and molecules in pore spaces or onto the external surfaces of clay crystals
405 (Garfinkel-Shweky and Yariv, 1997; Ransom et al., 1997; Ding et al., 2013; Lu et al.,

406 2013); that is, the bonding mode of OM and clay minerals in the dark mudstone changed
407 at the depth of 3100 m. Consequently, the illitization of smectite was liberated from the
408 pillar effect of interlayer OM.

409 OM, particularly fatty acids, can be well preserved in the nanopores of clay minerals
410 during sedimentation. Furthermore, because fatty acids can be adsorbed in the interlayer
411 spaces of smectite due to their improved resistance to oxidation and degradation
412 (Schulten et al., 1996; Salmon et al., 2000; Jandl et al., 2004), they can be desorbed into
413 the pore fluid, thereby releasing organic acids during diagenesis. Research on the source
414 rocks of the Dongying Depression has demonstrated that the threshold for OM thermal
415 evolution and hydrocarbon generation was 3000 m and the hydrocarbon generation peak
416 occurred at about 3200 m (Zhang et al., 2009). Surdam (1989) pointed out that kerogen
417 may produce large volumes of water-souble organic acid anions and phenols during the
418 maturation of OM in source rocks. However, the organic acid anions could typically
419 dominate pH of the waters and significantly affecting the stability of both carbonates and
420 aluminosilicates at the temperature of 80°C–120°C. This was consistent with the depth
421 range for the hydrocarbon generation in the Dongying Depression. Thus, it is proposed
422 that in our studied samples below 3100 m, OM became completely mature, discharging
423 abundant hydrocarbons and organic acids and causing a change in the pore water
424 composition and dissolution of inorganic minerals. Under these conditions,
425 potassium-rich minerals (Schmidt and McDonald, 1979; Bevan and Savage, 1989; Welch
426 and Ullman, 1993; Wilkinson and Haszeldine, 1996; Taylor et al., 2010), smectite
427 silicon-oxygen tetrahedra, and aluminum-oxygen octahedra (Huang and Keller, 1971;
428 Tan, 1986; Golubev et al., 2006; Pokrovsky et al., 2009) can be dissolved, thereby

429 catalyzing smectite dissolution and subsequent recrystallization to illite (Altaner, 1986;
430 Andresen et al., 1993; Small, 1994; Lanson et al., 2002; Golubev et al., 2006). In addition,
431 Berger et al. (1997) suggested that the maturation of OM may speed up the conversion
432 rate of smectite to illite by increasing the Gibbs Free Energy of illite growth. Generally,
433 below 3100 m this dissolution-recrystallization mechanism promoted the progression of
434 smectite illitization in the dark mudstone.

435 **IMPLICATIONS**

436 The disparities of smectite illitization between dark and red mudstones at the same
437 basin are largely due to the existence/absence of OM in the two systems, that is, the
438 water-rock system (red mudstone) and the water-rock-OM system (dark mudstone). The
439 staged evolution of clay minerals in dark mudstone is related to the occurrence transition
440 of OM. In general, the existence and occurrence of OM significantly affect the process of
441 smectite illitization. Thus more attention should be paid to the interactions of OM and
442 clay minerals to promote the understanding on the mechanism of smectite illitization and
443 thereby its geological applications such as geothermometer and hydrocarbon generation.

444 **ACKNOWLEDGMENTS**

445 This work was financed by the National Natural Science Foundation of China (Grant
446 No. 41072089; 41372130) and the National Oil and Gas Special Fund (Grant
447 No.2011ZX05006–001). We acknowledge Yuanfeng Cai, Tong He, and Yuguan Pan (all
448 in Nanjing) for their assistance with the X-ray diffraction and infrared spectroscopy. We
449 are thankful to Hejing Wang (Beijing) for his help with the crystallinity analyses. Meng
450 Xu (Shanghai) is thanked for providing assistance with the laboratory work.

REFERENCES

Ahn, J., and Peacor, D. (1986) Transmission and analytical electron microscopy of the smectite-to-illite transition. Clays and Clay Minerals, 34, 165-179.

Alstadt, K.N., Katti, D.R., and Katti, K.S. (2012) An in situ FTIR step-scan photoacoustic investigation of kerogen and minerals in oil shale. Spectrochimica Acta Part A: Molecular and Biomolecular Spectroscopy, 89, 105-113.

Altaner, S. (1986) Comparison of rates of smectite illitization with rates of K-feldspar dissolution. Clays and Clay Minerals, 34, 608-611.

Altaner, S., and Ylagan, R. (1997) Comparison of structural models of mixed-layer illite/smectite and reaction mechanisms of smectite illitization. Clays and Clay Minerals, 45, 517-533.

Andresen, B., Barth, T., and Throndsen, T. (1993) Generation potential of carbon dioxide and organic acids from North Sea source rocks: yields and carbon isotopic composition. In K. Øygard, Ed, Organic geochemistry: Poster Sessions from the 16th International Meeting on Organic Geochemistry, p. 281-284. Falch Hurtigtrykk (in Norwegian), Stavanger.

Balsam, W.L., and Deaton, B.C. (1991) Sediment dispersal in the Atlantic Ocean: evaluation by visible light spectra. Reviews in Aquatic Sciences, 4, 411-447.

Barker, C. (1980) Primary migration: the importance of water-mineral-organic matter interactions in the source rock. In W.H. Roberts, and R.J. Cordell, Eds. Problems of Petroleum Migration, 10, p. 19-31. American Association of Petroleum

Geologists, Tulsa, Oklahoma.

Baronnet, A. (1997) Silicate microstructures at the sub-atomic scale. Comptes rendus de l'Académie des sciences. Série 2. Sciences de la terre et des planètes (in French), 324, 157-172.

Barth, T., and Bjørlykke, K. (1993) Organic acids from source rock maturation: generation potentials, transport mechanisms and relevance for mineral diagenesis. Applied Geochemistry, 8, 325-337.

Barth, T., Borgund, A.E., Hopland, A.L., and Graue, A. (1988) Volatile organic acids produced during kerogen maturation—amounts, composition and role in migration of oil. Organic Geochemistry, 13, 461-465.

Bergaya, F., Theng, B.K., and Lagaly, G. (2011) Handbook of Clay Science, 1246 p. Elsevier, Amsterdam.

Berger, G., Lacharpagne, J.C., Velde, B., Beaufort, D., and Lanson, B. (1997) Kinetic constraints on illitization reactions and the effects of organic diagenesis in sandstone/shale sequences. Applied Geochemistry, 12, 23-35.

Bethke, C.M., and Altaner, S. (1986) Layer-by-layer mechanism of smectite illitization and application to a new rate law. Clays and Clay Minerals, 34, 136-145.

Bevan, J., and Savage, D. (1989) The effect of organic acids on the dissolution of K-feldspar under conditions relevant to burial diagenesis. Mineralogical Magazine, 53, 415-425.

Bobos, I., and Eberl, D. (2013) Thickness distributions and evolution of growth

493 mechanisms of NH_4-illite from the fossil hydrothermal system of Harghita Bãi,
494 Eastern Carpathians, Romania. Clays and Clay Minerals, 61, 375-391.
495 Boles, J.R., and Franks, S.G. (1979) Clay diagenesis in Wilcox sandstones of southwest
496 Texas: implications of smectite diagenesis on sandstone cementation. Journal of
497 Sedimentary Research, 49, 55-70.
498 Bourdelle, F., Parra, T., Beyssac, O., Chopin, C., and Vidal, O. (2013) Clay minerals as
499 geo-thermometer: A comparative study based on high spatial resolution analyses
500 of illite and chlorite in Gulf Coast sandstones (Texas, USA). American
501 Mineralogist, 98, 914-926.
502 Brtáňová, A., Madejová, J., Bizovská, V., and Komadel, P. (2014) Utilization of near
503 infrared spectroscopy for studying solvation properties of Cu-montmorillonites.
504 Spectrochimica Acta Part A: Molecular and Biomolecular Spectroscopy, 123,
505 385-391.
506 Bruce, C.H. (1984) Smectite dehydration-its relation to structural development and
507 hydrocarbon accumulation in northern Gulf of Mexico Basin. AAPG Bulletin, 68,
508 673-683.
509 Burst, J.F. (1969) Diagenesis of Gulf Coast clayey sediments and its possible relation to
510 petroleum migration. AAPG Bulletin, 53, 73-93.
511 Cai, J. (2004) Organic-Complexes in Muddy Sediment and Mudstone, 212 p. Science
512 Press, Beijing.
513 Cai, J., Bao, Y., Yang, S., Wang, X., Fan, D., Xu, J., and Wang, A. (2007) Research on

preservation and enrichment mechanisms of organic matter in muddy sediment and mudstone. Science in China Series D: Earth Sciences, 50, 765-775.

Cai, J., Lu, L., Bao, Y., Fan, F., and Xu, J. (2011) The significance and variation characteristics of interlay water in smectite of hydrocarbon source rocks. Science in China Series D: Earth Sciences, 42, 1-8.

Cai, J., Song, M., Lu, L., Bao, Y., Ding, F., and Xu, J. (2013) Organo-clay complexes in source rocks—a natural material for hydrocarbon generation. Marine Geology and Quaternary Geology, 33, 123-131.

Clausen, P., Meier, L., Hughes, E., Plummer, C.J., and Månson, J.-A.E. (2013) Kinetics of desorption of water, ethanol, ethyl acetate, and toluene from a montmorillonite. Clays and Clay Minerals, 61, 361-374.

Colombo, C., and Violante, A. (1997) Effect of ageing on the nature and interlayering of mixed hydroxy Al-Fe-montmorillonite complexes. Clay Minerals, 32, 55-64.

Cuadros, J. (2012) Clay crystal-chemical adaptability and transformation mechanisms. Clay Minerals, 47, 147-164.

Cuadros, J., and Altaner, S.P. (1998) Compositional and structural features of the octahedral sheet in mixed-layer illite/smectite from bentonites. European Journal of Mineralogy, 10, 111-124.

Cuadros, J., and Linares, J. (1996) Experimental kinetic study of the smectite-to-illite transformation. Geochimica et Cosmochimica Acta, 60, 439-453.

Dias, R.F., Freeman, K.H., Lewan, M.D., and Franks, S.G. (2002) ^{13}C of

low-molecular-weight organic acids generated by the hydrous pyrolysis of oil-prone source rocks. Geochimica et Cosmochimica Acta, 66, 2755-2769.

Ding, F., Cai, J., Song, M., and Yuan, P. (2013) The relationship between organic matter and specific surface area in <2 μm clay size fraction of muddy source rock. Science in China Series D: Earth Sciences, 56, 1343-1349.

Dong, H., Jaisi, D.P., Kim, J., and Zhang, G. (2009) Microbe-clay mineral interactions. American Mineralogist, 94, 1505-1519.

Drits, V.A., Lindgreen, H., and Salyn, A.L. (1997) Determination of the content and distribution of fixed ammonium in illite-smectite by X-ray diffraction: Application to North Sea illite-smectite. American Mineralogist, 82, 79-87.

Eberl, D., and Hower, J. (1976) Kinetics of illite formation. Geological Society of America Bulletin, 87, 1326-1330.

Eberl, D., and Srodon, J. (1988) Ostwald ripening and interparticle-diffraction effects for illite crystals. American Mineralogist, 73, 1335-1345.

Eberl, D., Velde, B., and McCormick, T. (1993) Synthesis of illite-smectite from smectite at earth surface temperatures and high pH. Clay Minerals, 28, 49-49.

Feng, Y., Li, S., and Lu, Y. (2013) Sequence stratigraphy and architectural variability in Late Eocene lacustrine strata of the Dongying Depression, Bohai Bay Basin, Eastern China. Sedimentary Geology, 295, 1-26.

Ganor, J., Reznik, I.J., and Rosenberg, Y.O. (2009) Organics in water-rock interactions. Reviews in mineralogy and geochemistry, 70, 259-369.

556 Garfinkel-Shweky, D., and Yariv, S. (1997) Metachromasy in clay-dye systems: the
557 adsorption of acridine orange by Na-saponite. Clay Minerals, 32, 653-663.
558 Ge, Y., Liu, L., and Ji, J. (2009) Rapid quantification of calcite in North Atlantic
559 sediments by DRIFTS and its climate significance-example of drilling site U1308.
560 Geological Journal of China Universities, 15, 184-191.
561 Golubev, S.V., Bauer, A., and Pokrovsky, O.S. (2006) Effect of pH and organic ligands on
562 the kinetics of smectite dissolution at 25°C. Geochimica et Cosmochimica Acta,
563 70, 4436-4451.
564 Grim, R.E. (1953) Clay Mineralogy, 596 p. McGraw-Hill, New York.
565 Guan, P., and Xu, C. (1998) Different occurrences of OM and its quantative estimation in
566 argillaceous source rocks. Chinese Science Bulletin, 43, 1556-1559.
567 He, H., and Guo, J. (2001) An experimental study of adsorption capacity of
568 montmorillonite, kaolinite and illite for heavy metals. Acta Petrologica Et
569 Mineralogica, 20, 573-578.
570 Howard, J.J., and Roy, D. (1985) Development of layer charge and kinetics of
571 experimental smectite alteration. Clays and Clay Minerals, 33, 81-88.
572 Hower, J., Eslinger, E.V., Hower, M.E., and Perry, E.A. (1976) Mechanism of burial
573 metamorphism of argillaceous sediment: 1. Mineralogical and chemical evidence.
574 Geological Society of America Bulletin, 87, 725-737.
575 Huang, W., and Keller, W. (1971) Dissolution of clay minerals in dilute organic acids at
576 room temperature. American Mineralogist, 56, 1082-1095.

Huang, W.L., Longo, J.M., and Pevear, D.R. (1993) An experimentally derived kinetic model for smectite-to-illite conversion and its use as a geothermometer. Clays and Clay Minerals, 41, 162-162.

Jandl, G., Leinweber, P., Schulten, H.R., and Eusterhues, K. (2004) The concentrations of fatty acids in organo-mineral particle-size fractions of a Chernozem. European journal of soil science, 55, 459-470.

Kennedy, M.J., Pevear, D.R., and Hill, R.J. (2002) Mineral surface control of organic carbon in black shale. Science, 295, 657-660.

Kim, J. (2012) Overviews of biogenic smectite-to-illite reaction. Clay Science, 16, 9-13.

Kim, J., Dong, H., Seabaugh, J., Newell, S.W., and Eberl, D.D. (2004) Role of microbes in the smectite-to-illite reaction. Science, 303, 830-832.

Lanson, B., Beaufort, D., Berger, G., Bauer, A., Cassagnabere, A., and Meunier, A. (2002) Authigenic kaolin and illitic minerals during burial diagenesis of sandstones: a review. Clay Minerals, 37, 1-22.

Lanson, B., Sakharov, B.A., Claret, F., and Drits, V.A. (2009) Diagenetic smectite-to-illite transition in clay-rich sediments: A reappraisal of X-ray diffraction results using the multi-specimen method. American Journal of Science, 309, 476-516.

Lei, Y., Luo, X., Song, G., Zhang, L., Hao, X., Yang, W., Song, P., Cheng, M., and Yang, B. (2014) Quantitative Characterization of Connectivity and Conductivity of Sandstone Carriers during Secondary Petroleum Migration, applied to the Third Member of Eocene Shahejie Formation, Dongying Depression, Eastern China.

598 Marine and Petroleum Geology, 51, 268-285.

599 Lewan, M., and Fisher, J. (1994) Organic acids from petroleum source rocks. In E.D.
600 Pittman, and M.D. Lewan, Eds. Organic Acids in Geological Processes, p. 70-114.
601 Springer Berlin Heidelberg, Berlin.

602 Li, J., and David, J.B. (2005) Palynofacies: principles and methods. Acta Palaeontologica
603 Sinica, 44, 138-156.

604 Liu, D., Dong, H., Zhao, L., and Wang, H. (2014) Smectite reduction by Shewanella
605 species as facilitated by cystine and cysteine. Geomicrobiology Journal, 31,
606 53-63.

607 Lu, L., Cai, J., Liu, W., Teng, E., and Wang, J. (2013) Occurrence and thermostability of
608 absorbed organic matter on clay minerals in mudstones and muddy sediments. Oil
609 and Gas Geology, 34, 16-26.

610 Lu, X., Hu, W., Fu, Q., Miao, D., Zhou, G., and Hong, Z. (1999) Study of combination
611 pattern of soluble organic matters and clay minerals in the immature source rocks
612 in Dongying Depression, China. Scientia Geologica Sinica, 34, 72-80.

613 Madejová, J., Pálková, H., Pentrák, M., and Komadel, P. (2009) Near-infrared
614 spectroscopic analysis of acid-treated organo-clays. Clays and Clay Minerals, 57,
615 392-403.

616 Moore, D.M., and Reynolds, R.C. (1997) X-Ray Diffraction and the Identification and
617 Analysis of Clay Minerals, 332 p. Oxford University Press, New York.

618 Mortland, M. (1970) Clay-organic complexes and interactions. Advances in Agronomy,

22, 75-117.

Mosser-Ruck, R., Cathelineau, M., Baronnet, A., and Trouiller, A. (1999) Hydrothermal reactivity of K-smectite at 300C and 100 bar: dissolution-crystallization process and non-expandable dehydrated smectite formation. Clay Minerals, 34, 275-290.

Mosser-Ruck, R., Pironon, J., Cathelineau, M., and Trouiller, A. (2001) Experimental illitization of smectite in a K-rich solution. European Journal of Mineralogy, 13, 829-840.

Nadeau, P., Wilson, M., McHardy, W., and Tait, J. (1985) The conversion of smectite to illite during diagenesis: evidence from some illitic clays from bentonites and sandstones. Mineralogical Magazine, 49, 393-400.

Naranjo, P.M., Sham, E.L., Castellón, E.R., Sánchez, R.M.T., and Torres, E.M.F. (2013) Identification and quantification of the interaction mechanisms between the cationic surfactant HDTMA-Br and montmorillonite. Clays and Clay Minerals, 61, 98-106.

Nemecz, E. (1981) Clay Minerals, 547 p. Akademiai Kiado, Budapest.

Nguyen, T., Janik, L.J., and Raupach, M. (1991) Diffuse reflectance infrared Fourier transform (DRIFT) spectroscopy in soil studies. Soil Research, 29, 49-67.

Occelli, M., and Tindwa, R. (1983) Physicochemical properties of montmorillonite interlayered with cationic oxyaluminum pillars. Clays and Clay Minerals, 31, 22-28.

Olives, J., Amouric, M., and Perbost, R. (2000) Mixed layering of illite-smectite: Results

from high-resolution transmission electron microscopy and lattice-energy calculations. Clays and Clay Minerals, 48, 282-289.

Pacton, M., Gorin, G.E., and Vasconcelos, C. (2011) Amorphous organic matter—Experimental data on formation and the role of microbes. Review of Palaeobotany and Palynology, 166, 253-267.

Pascual, J., Corpas, F., López-Beceiro, J., Benítez-Guerrero, M., and Artiaga, R. (2009) Thermal characterization of a Spanish red mud. Journal of thermal analysis and calorimetry, 96, 407-412.

Pentrák, M., Bizovská, V., and Madejová, J. (2012) Near-IR study of water adsorption on acid-treated montmorillonite. Vibrational Spectroscopy, 63, 360-366.

Pentráková, L., Su, K., Pentrák, M., and Stucki, J. (2013) A review of microbial redox interactions with structural Fe in clay minerals. Clay Minerals, 48, 543-560.

Perry, E.A., and Hower, J. (1972) Late-stage dehydration in deeply buried pelitic sediments. AAPG Bulletin, 56, 2013-2021.

Pevear, D.R. (1999) Illite and hydrocarbon exploration. Proceedings of the National Academy of Sciences, 96, 3440-3446.

Pokrovsky, O., Golubev, S., and Jordan, G. (2009) Effect of organic and inorganic ligands on calcite and magnesite dissolution rates at 60°C and 30 atm pCO_2. Chemical Geology, 265, 33-43.

Pollard, C.O. (1971) Appendix: Semidisplacive mechanism for diagenetic alteration of montmorillonite layers to illite layers. Geological Society of America Special

661 Papers, 134, 79-94.

662 Pollastro, R.M. (1993) Considerations and applications of the illite/smectite
663 geothermometer in hydrocarbon-bearing rocks of Miocene to Mississippian age.
664 Clays and Clay Minerals, 41, 119-119.

665 Pusino, A., Liu, W., and Gessa, C. (1993) Dimepiperate adsorption and hydrolysis on Al^{3+},
666 Fe^{3+}, Ca^{2+}, and Na^{+} montmorillonite. Clays and Clay Minerals, 41, 335-340.

667 Putnis, A. (2002) Mineral replacement reactions: from macroscopic observations to
668 microscopic mechanisms. Mineralogical Magazine, 66, 689-708.

669 Pytte, A., and Reynolds, R. (1989) The thermal transformation of smectite to illite. In
670 N.D. Naeser, and T.H. McCulloh, Eds. Thermal History of Sedimentary Nasins, p.
671 133-140. Springer, New York.

672 Ransom, B., Bennett, R.H., Baerwald, R., and Shea, K. (1997) TEM study of in situ
673 organic matter on continental margins: occurrence and the “monolayer”
674 hypothesis. Marine Geology, 138, 1-9.

675 Reynolds, R.C., Jr. (1985) NEWMOD, a computer program for the calculation of
676 one-dimensional diffraction patterns of mixed-layered clays. RC Reynolds.
677 Hanover, New Hampshire.

678 Roberson, H.E., and Lahann, R.W. (1981) Smectite to illite conversion rates: effects of
679 solution chemistry. Clays and Clay Minerals, 29, 129-135.

680 Russell, J., and Farmer, V. (1964) Infra-red spectroscopic study of the dehydration of
681 montmorillonite and saponite. Clay Minerals Bulletin, 5, 443-464.

682 Salmon, V., Derenne, S., Lallier-Vergès, E., Largeau, C., and Beaudoin, B. (2000)
683 Protection of organic matter by mineral matrix in a Cenomanian black shale.
684 Organic Geochemistry, 31, 463-474.
685 Schmidt, V., and McDonald, D.A. (1979) The role of secondary porosity in the course of
686 sandstone diagenesis. The Society of Economic Paleontologists and Mineralogists,
687 26, 175-207.
688 Schulten, H.-R., Leinweber, P., and Theng, B. (1996) Characterization of organic matter
689 in an interlayer clay-organic complex from soil by pyrolysis methylation-mass
690 spectrometry. Geoderma, 69, 105-118.
691 Schumann, D., Hartman, H., Eberl, D.D., Sears, S.K., Hesse, R., and Vali, H. (2013) The
692 influence of oxalate-promoted growth of saponite and talc crystals on rectorite:
693 Testing the intercalation-synthesis hypothesis of 2: 1 layer silicates. Clays and
694 Clay Minerals, 61, 342-360.
695 Small, J. (1994) Fluid composition, mineralogy and morphological changes associated
696 with the smectite-to-illite reaction; an experimental investigation of the effect of
697 organic acid anions. Clay Minerals, 29, 539-554.
698 Speight, J.G. (1999) The Chemistry and Technology of Petroleum, 953 p. Marcel Dekker,
699 New York.
700 Środoń, J. (1999) Use of clay minerals in reconstructing geological processes; recent
701 advances and some perspectives. Clay Minerals, 34, 27-37.
702 Środoń, J., Clauer, N., Huff, W., Dudek, T., and Banaś, M. (2009) K-Ar dating of the

703 Lower Palaeozoic K-bentonites from the Baltic Basin and the Baltic Shield:
704 implications for the role of temperature and time in the illitization of smectite.
705 Clay Minerals, 44, 361-387.
706 Tan, K.H. (1986) Degradation of soil minerals by organic acids. In P.M. Huang, and M.
707 Schnitzer, Eds. Interactions with Soil Minerals with Natural Organics and
708 Microbes, 17, p. 1-27. Soil Science Society of America, Madison, Wisconsin,
709 U.S.A.
710 Taylor, T.R., Giles, M.R., Hathon, L.A., Diggs, T.N., Braunsdorf, N.R., Birbiglia, G.V.,
711 Kittridge, M.G., Macaulay, C.I., and Espejo, I.S. (2010) Sandstone diagenesis and
712 reservoir quality prediction: Models, myths, and reality. AAPG bulletin, 94,
713 1093-1132.
714 Theng, B.K.G. (1974) The Chemistry of Clay-Organic Reactions, 343 p. Wiley, New
715 York
716 ---. (1979) Formation and Properties of Clay-Polymer Complexes, 362 p. Elsevier,
717 Amsterdam.
718 Theng, B.K.G., Churchman, G., and Newman, R. (1986) The occurrence of interlayer
719 clay-organic complexes in two New Zealand soils. Soil Science, 142, 262-266.
720 Tissot, B., and Welte, D. (1984) Petroleum Formation and Occurrence: A New Approach
721 to Oil and Gas Exploration, 699 p. Springer, Berlin.
722 Tyson, R.V. (1993) Palynofacies analysis In D.G. Jenkins, Ed. Applied
723 Micropalaeontology, p. 153-191. Springer, Netherlands.

Ugochukwu, U.C., Jones, M.D., Head, I.M., Manning, D.A., and Fialips, C.I. (2013) Effect of acid activated clay minerals on biodegradation of crude oil hydrocarbons. International Biodeterioration & Biodegradation.

Weaver, C.E., and Pollard, L.D. (1973) The chemistry of clay minerals, 213 p. Elsevier, Amsterdam.

Welch, S.A., and Ullman, W.J. (1993) The effect of organic acids on plagioclase dissolution rates and stoichiometry. Geochimica et Cosmochimica Acta, 57, 2725-2736.

Whitney, G. (1990) Role of water in the smectite-to-illite reaction. Clays and Clay Minerals, 38, 343-350.

Whitney, G., and Velde, B. (1993) Changes in particle morphology during illitization; an experimental study. Clays and Clay Minerals, 41, 209-218.

Wilkinson, M., and Haszeldine, R.S. (1996) Aluminium loss during sandstone diagenesis. Journal of the Geological Society, 153, 657-660.

Xiong, Y., Xu, Y., and Chen, J. (1983) Soil Colloid (Material Basis of Soil Colloid), 440 p. Science Press, Beijing.

Yariv, S., and Cross, H. (2002) Organo-Clay Complexes and Interactions, 688 p. Dekker, New York.

Yariv, S., and Lapides, I. (2005) The use of thermo-XRD-analysis in the study of organo-smectite complexes. Journal of thermal analysis and calorimetry, 80, 11-26.

Yu, B., Dong, H., and Han, P. (2012) Experimental research on microbial degradation of organic matter adsorbed in smectite internal surface area in the interlayer of the structure. Acta Petrologica Sinica, 28, 949-960.

Yu, W.H., Li, N., Tong, D.S., Zhou, C.H., Lin, C.X.C., and Xu, C.Y. (2013) Adsorption of proteins and nucleic acids on clay minerals and their interactions: A review. Applied Clay Science, 80, 443-452.

Zhang, G., Dong, H., Kim, J., and Eberl, D. (2007a) Microbial reduction of structural Fe3+ in nontronite by a thermophilic bacterium and its role in promoting the smectite to illite reaction. American Mineralogist, 92, 1411-1419.

Zhang, G., Kim, J., Dong, H., and Sommer, A.J. (2007b) Microbial effects in promoting the smectite to illite reaction: Role of organic matter intercalated in the interlayer. American Mineralogist, 92, 1401-1410.

Zhang, L., Liu, Q., Zhu, R., Li, Z., and Lu, X. (2009) Source rocks in Mesozoic–Cenozoic continental rift basins, east China: a case from Dongying Depression, Bohai Bay Basin. Organic Geochemistry, 40, 229-242.

Figure captions

765 **Figure 1.** Location map. (**a**) Study area in the Dongying Depression, Bohai Bay Basin,
766 China. The red box denotes the Dongying Depression. (**b**) Structural map of the
767 Dongying Depression with locations of sampled wells, modified after Zhang et al. (2009).

768 **Figure 2.** Scatter diagrams of clay mineral proportions and N_{ave} of I-S in <2-μm fractions
769 of red and dark mudstones with depth. (**a**), illite; (**b**), I-S and smectite; (**c**), kaolinite; (**d**),
770 chlorite; (**e**), illite percentage in I-S; (**f**), N_{ave} of I-S. N_{ave} denotes the average number of
771 layers in the stacking sequence of the I-S.

772 **Figure 3.** XRD patterns of ethylene glycol-saturated specimens of <2-μm fractions from
773 red (**a**) and dark (**b**) mudstone samples. The Reichweite (R) values of the I-S were
774 determined using the method from Moore and Reynolds (1997) and the computer
775 program NEWMOD 2.0 (Reynolds, 1985).

776 **Figure 4.** Variation of Stacking mode of I-S with depth in <2-μm fractions from red and
777 dark mudstone samples.

778 **Figure 5.** Variation of TOC content of the studied samples with depth. TOC of the red
779 mudstones (**a**) ranged from 0.01% to 0.14%, whereas that in the dark mudstones (**b**)
780 raged from 0.17% to 4.43%.

781 **Figure 6.** Variations of d_{001} diffraction of I-S in <2-μm fractions under air-dried, 250°C
782 and 550°C heated from red (**a**) and dark (**b**) mudstone samples. The d_{001} peak values were
783 determined using Jade 6.5 program (Materials Data, Inc.).

784 **Figure 7.** X-ray diffraction patterns of <2-μm fractions from the red (**a**) and dark (**b**)
785 mudstone samples heated to 250°C (solid line) and 550°C (dotted line).

786 **Figure 8.** The MIR spectra of <2-μm fractions from red (**a**) and dark (**b**) mudstone
787 samples located in the 2700-3100-cm^{-1} region. The samples of dark mudstones (**b**) show
788 distinct C-H vibrations (3050 cm^{-1}, 2926 cm^{-1}, and 2854 cm^{-1}) whereas samples of red
789 mudstones (**a**) show distortions of CO_3^{2-} stretching vibrations (2980 cm^{-1}).

790 **Figure 9.** NIR spectra of <2-μm fractions from red (**a**) and dark (**b**) mudstone samples.
791 The band near 7080 cm^{-1} consists of the first overtone of water molecules ($2\nu H_2O$) and
792 first overtone structural OH groups ($2\nu OH$). The band near 5250 cm^{-1} was related to the
793 combination of stretching and bending vibrations of water $(\nu+\delta)H_2O$. ν denotes the
794 stretching vibration, δ denotes the bending vibration.

795 **Figure 10.** Relationship between TOC content and peak area of the aliphatic CH_2
796 stretching vibration in the MIR spectra.

797 **Figure 11.** Variation with depth of peak area of the aliphatic CH_2 stretching vibration in
798 the MIR spectra of dark mudstone samples.

799

800
801

Table 1. Mineral data for the <2-μm fractions of the red and dark mudstone samples

Sample No.	Well	Depth (m)	Lithology	Mineral content (%)									Clay content (%)					I-S				TOC (%)
				Clay	Quartz	Potassium Feldspar	Plagioclase	Calcite	Dolomite	Anhydrite	Siderite	Pyrite	Kaolinite	Chlorite	Illite	Smectite	I-S	I %	Reichweite parameter	N	N_{ave}	
D03	H130	2245	grey mudstone	37	32	5	25	0	0	0	1	0	6	4	14	6	70	51	0	1-3	2	1.98
D01	Ch101	2291	dark grey mudstone	43	36	5	10	4	1	0	1	0	7	10	11	2	70	64	0	2-5	3.5	0.39
D02	Ch101	2357	grey mudstone	42	35	3	8	9	3	0	0	0	4	12	18	0	65	73	0.5	1-5	3	1.88
D07	W31	2507	dark grey and silty mudstone	26	21	0	12	35	3	0	3	0	12	3	27	0	58	77	0	1-8	4.5	1.67
D08	F4	2704	dark grey mudstone	37	29	0	12	19	0	0	2	1	20	4	15	6	54	61	0	0-5	2.5	2.14
D04	H130	2787	dark grey mudstone	38	28	2	8	22	0	0	2	0	14	5	21	0	60	75	0	0-7	3.5	1.81
D05	H130	2882	dark grey sandy mudstone	53	35	4	3	2	0	2	1	0	12	6	25	0	57	77	0.5	1-6	3.5	0.66
D09	F112	2905	massive mudstone	36	41	0	18	0	3	0	2	0	15	3	28	0	54	75	0	0-6	3	0.76
D22	H147	3032	dark grey mudstone	31	35	5	8	3	17	0	1	0	19	5	25	0	51	80	0.5	0-6	3	0.79
D23	H147	3042	dark grey and lime mudstone	39	41	5	6	5	0	2	2	0	17	6	19	0	57	80	0.5	0-6	3	2.52
D20	N872	3050	dark grey mudstone	33	25	0	6	30	1	0	2	3	8	4	32	0	55	78	0.5	0-6	3	2.62
D10	F112	3117	lamellar mudstone	23	16	0	4	52	1	0	2	2	24	7	57	0	12	83	1	2-8	5	2.95
D11	F112	3122	lamellar mudstone	23	18	0	4	49	3	0	1	2	12	8	66	0	14	83	1	1-9	5	2.84
D19	F137	3178	grey mudstone	38	30	0	12	7	6	0	6	1	0	0	87	0	13	87	1.5	0-8	4	0.17
D15	F120	3278	dark grey and silty limestone	13	16	0	4	58	9	0	0	0	0	0	88	0	12	85	0.5	0-10	5	2.05
D16	F120	3283	dark grey and silty limestone	16	18	0	5	42	16	0	0	3	0	0	70	0	30	85	0.5	1-8	4.5	3.34
D17	F120	3339	dark grey and silty limestone	31	41	0	10	7	7	0	4	0	1	5	87	0	6	87	1.5	2-8	5	0.18
D13	F112	3430	gypsiferous mudstone	17	24	0	6	40	13	0	0	0	0	0	83	0	17	90	1.5	4-12	8	4.43
D14	F112	3492	gypsiferous mudstone	26	23	0	13	0	32	5	1	0	0	0	91	0	9	90	3	0-11	5.5	1.37
R06	W135	995	red mudstone	49	27	3	11	10	0	0	0	0	22	14	4	49	10	30	0	0-6	3	0.01
R07	T271	1385	red mudstone	32	36	4	1	20	7	0	0	0	27	5	6	12	51	54	0	2-4	3	0.07
R08	Sh3-80	1466	red mudstone	74	19	4	0	2	1	0	0	0	6	3	2	20	69	27	0	0-4	2	0.03
R09	W100	1821	red mudstone	53	22	4	8	11	2	0	0	0	12	4	17	5	62	66	0	2-5	3.5	0.08
R10	W100	2118	red mudstone	37	34	4	14	11	0	0	0	0	7	3	16	0	74	76	0	3-6	4.5	0.04
R11	W100	2219	red mudstone	53	27	3	5	11	0	0	1	0	13	6	28	0	53	85	0.5	2-8	5	0.07
R12	W135	2845	red mudstone	48	27	3	10	11	0	0	1	0	4	7	60	0	29	83	0.5	2-7	4.5	0.1
R13	G112	3184	red mudstone	54	22	0	8	12	3	0	1	0	7	7	69	0	17	90	1.5	0-9	4.5	0.14
R14	Hk1	4022	red mudstone	46	24	0	14	13	3	0	0	0	6	16	68	0	10	90	1.5	4-9	6.5	0.11
R15	Hk1	4502	red mudstone	50	27	0	10	11	2	0	0	0	4	16	78	0	2	92	3	0-11	5.5	0.05
R16	Hk1	5271	red mudstone	41	30	0	15	13	0	0	1	0	5	16	72	0	7	92	3	0-11	5.5	0.06

Notes: I-S means mixed-layer illite-smectite. I % means illite proportion in I-S. N means range of number of layers in the stacking sequence of the I-S. N_{ave} means average number of layers in the stacking sequence of the I-S.

Figure 1

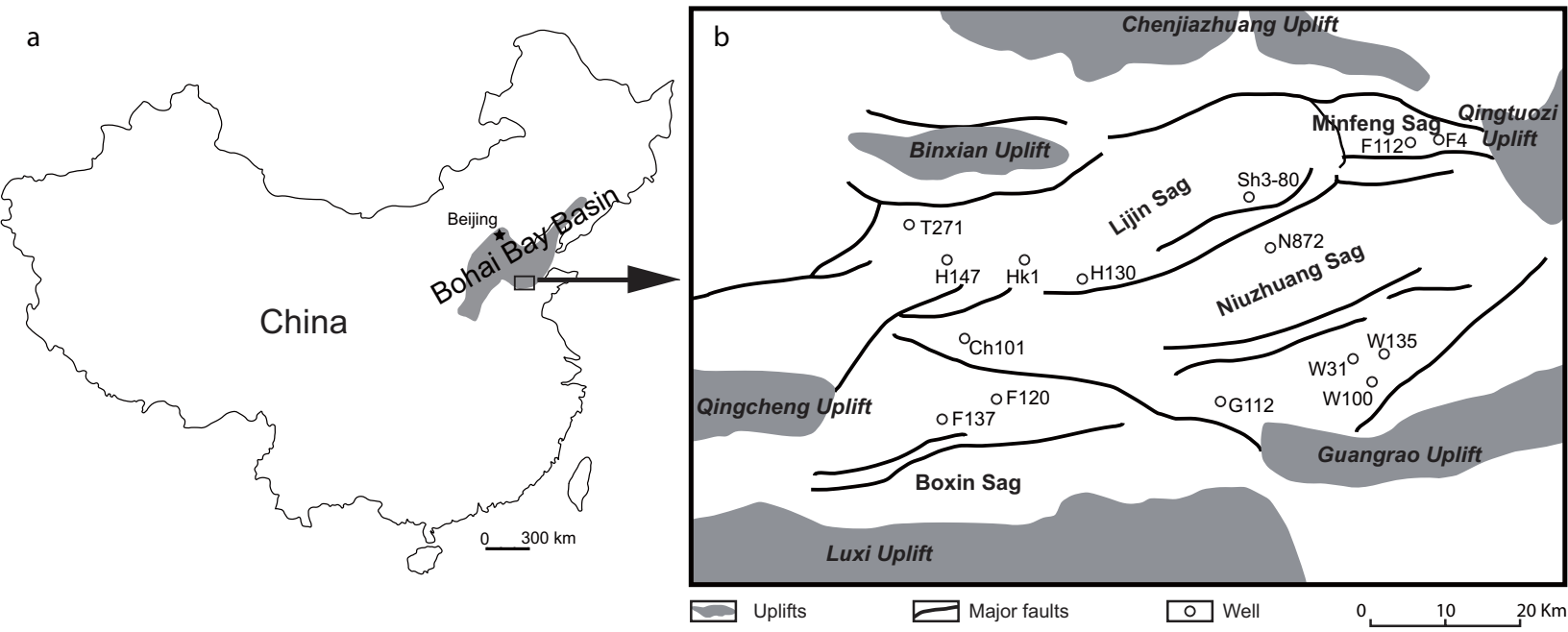
a
Beijing
Bohai Bay Basin
China
0 300 km
b
Chenjiazhuang Uplift
Binxian Uplift
Minfeng Sag
F112
F4
Qingtuozi Uplift
Sh3-80
Lijin Sag
T271
N872
H147
Hk1
H130
Niuzhuang Sag
Ch101
W135
W31
W100
F120
G112
Qingcheng Uplift
F137
Guangrao Uplift
Boxin Sag
Luxi Uplift
Uplifts
Major faults
Well
0 10 20 Km

Figure 2

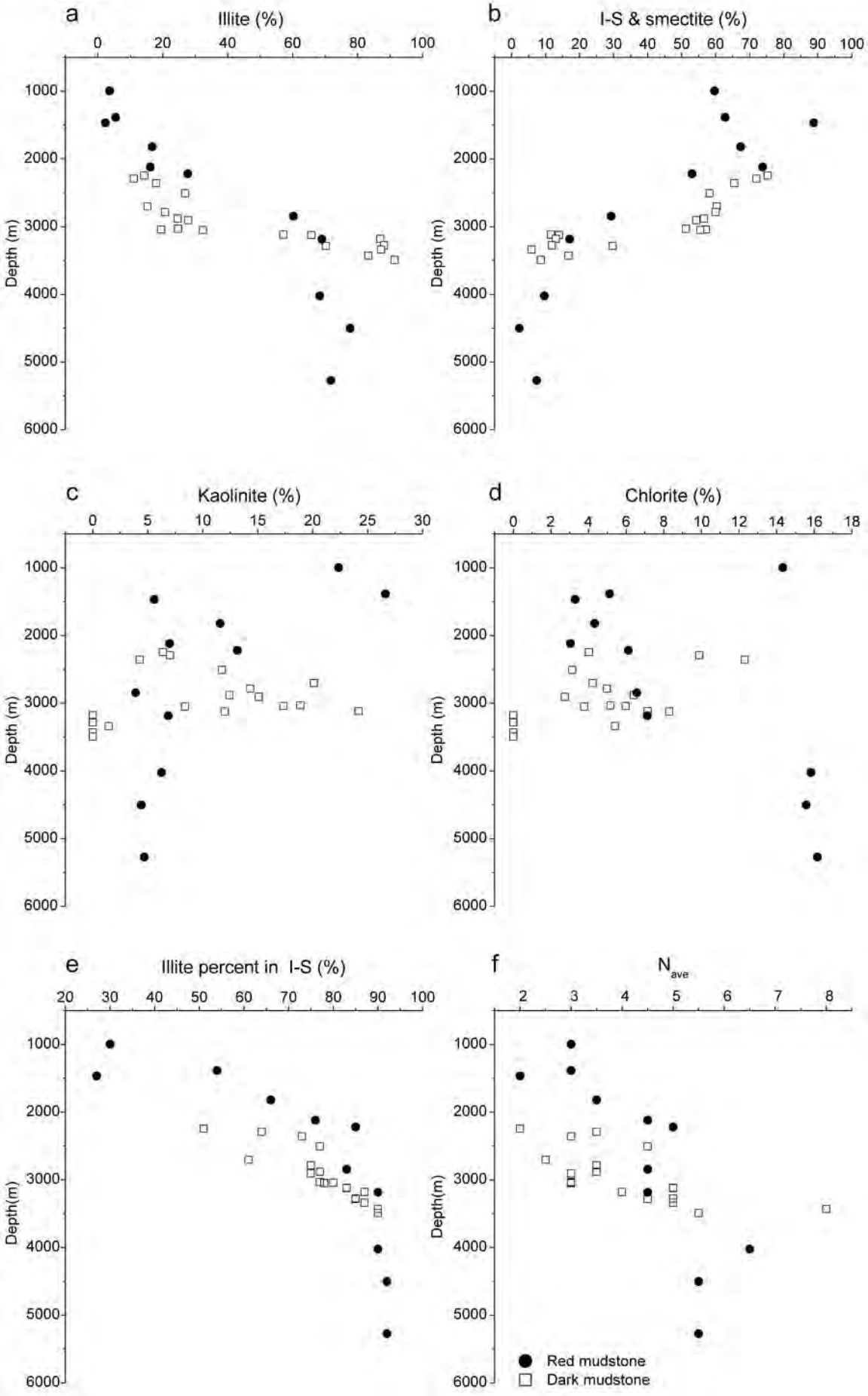
a
Illite (%)
0 20 40 60 80 100
b
I-S & smectite (%)
0 10 20 30 40 50 60 70 80 90 100
c
Kaolinite (%)
0 5 10 15 20 25 30
d
Chlorite (%)
0 2 4 6 8 10 12 14 16 18
e
Illite percent in I-S (%)
20 30 40 50 60 70 80 90 100
f
N_{ave}
2 3 4 5 6 7 8
Depth (m)
Depth(m)
1000 2000 3000 4000 5000 6000
Red mudstone
Dark mudstone

Figure 3

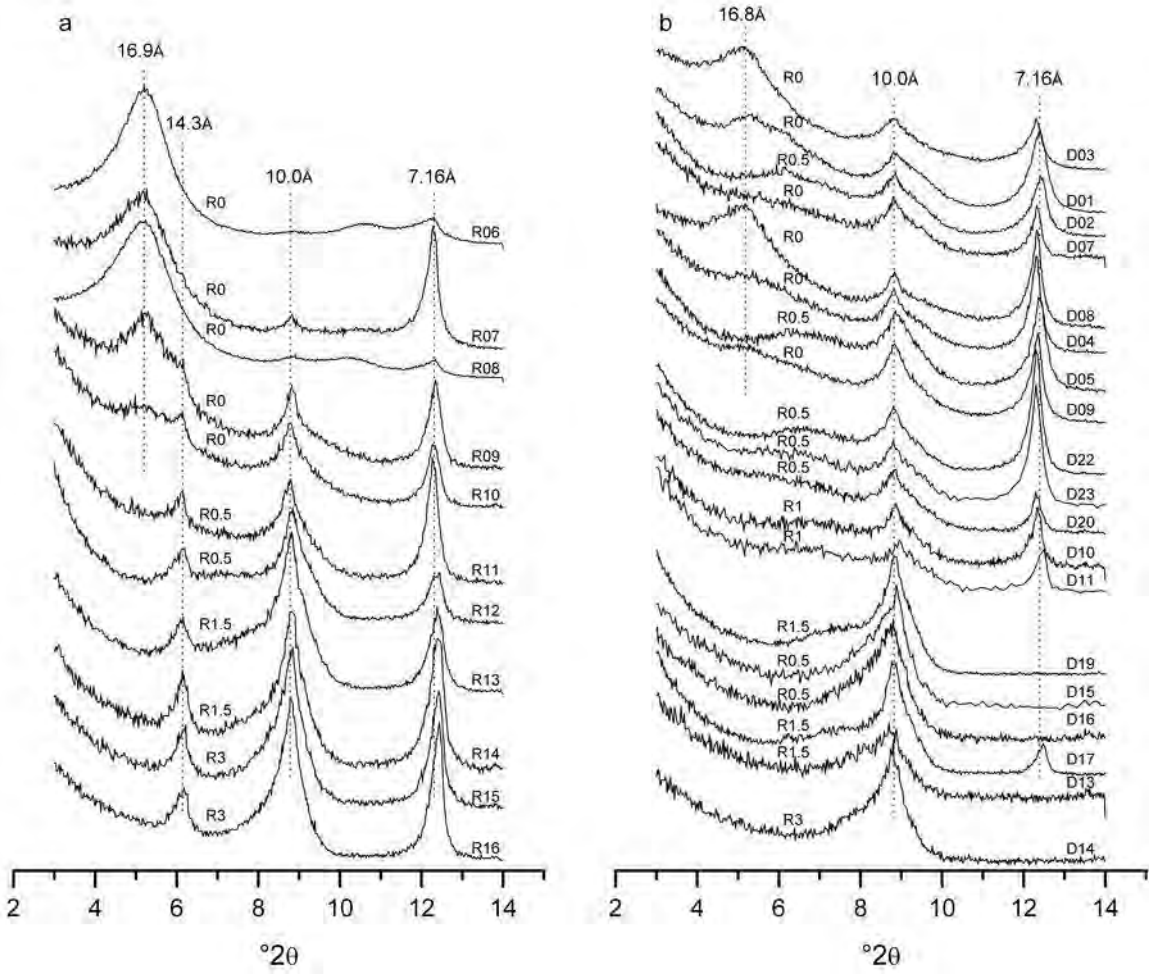
a
16.9Å
14.3Å
10.0Å
7.16Å
R0
R06
R0
R07
R0
R08
R0
R0
R09
R10
R0.5
R0.5
R11
R12
R1.5
R13
R1.5
R3
R14
R3
R15
R16
2
4
6
8
10
12
14
°2θ
b
16.8Å
10.0Å
7.16Å
R0
R0
R0.5
R0
R0
R0
R0.5
R0
R0.5
R0.5
R0.5
R1
R1
R1.5
R0.5
R0.5
R1.5
R1.5
R3
D03
D01
D02
D07
D08
D04
D05
D09
D22
D23
D20
D10
D11
D19
D15
D16
D17
D13
D14
2
4
6
8
10
12
14
°2θ

Figure 4

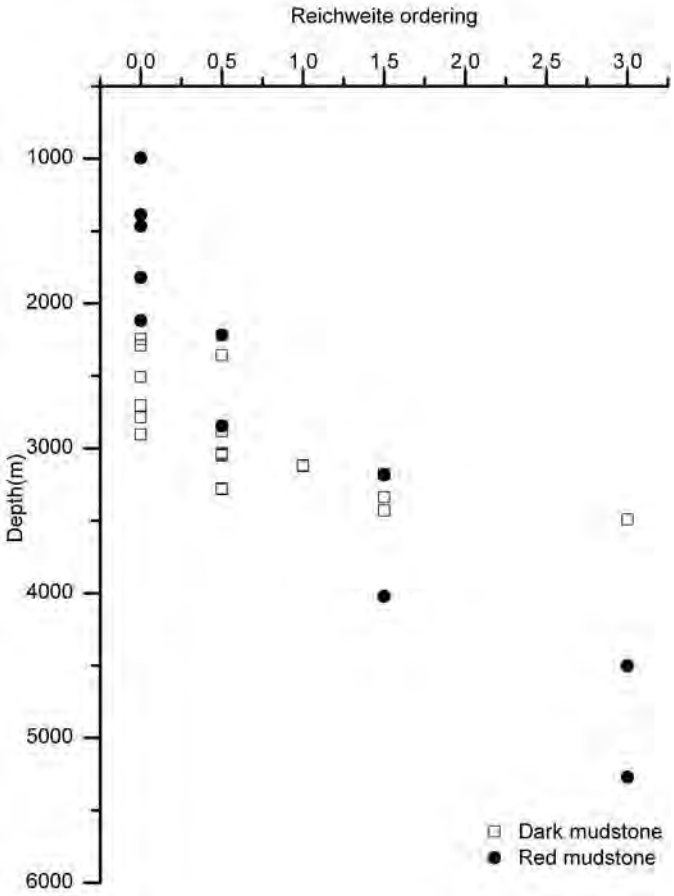
Reichweite ordering
0.0
0.5
1.0
1.5
2.0
2.5
3.0
1000
2000
3000
4000
5000
6000
Depth(m)
Dark mudstone
Red mudstone

Figure 5

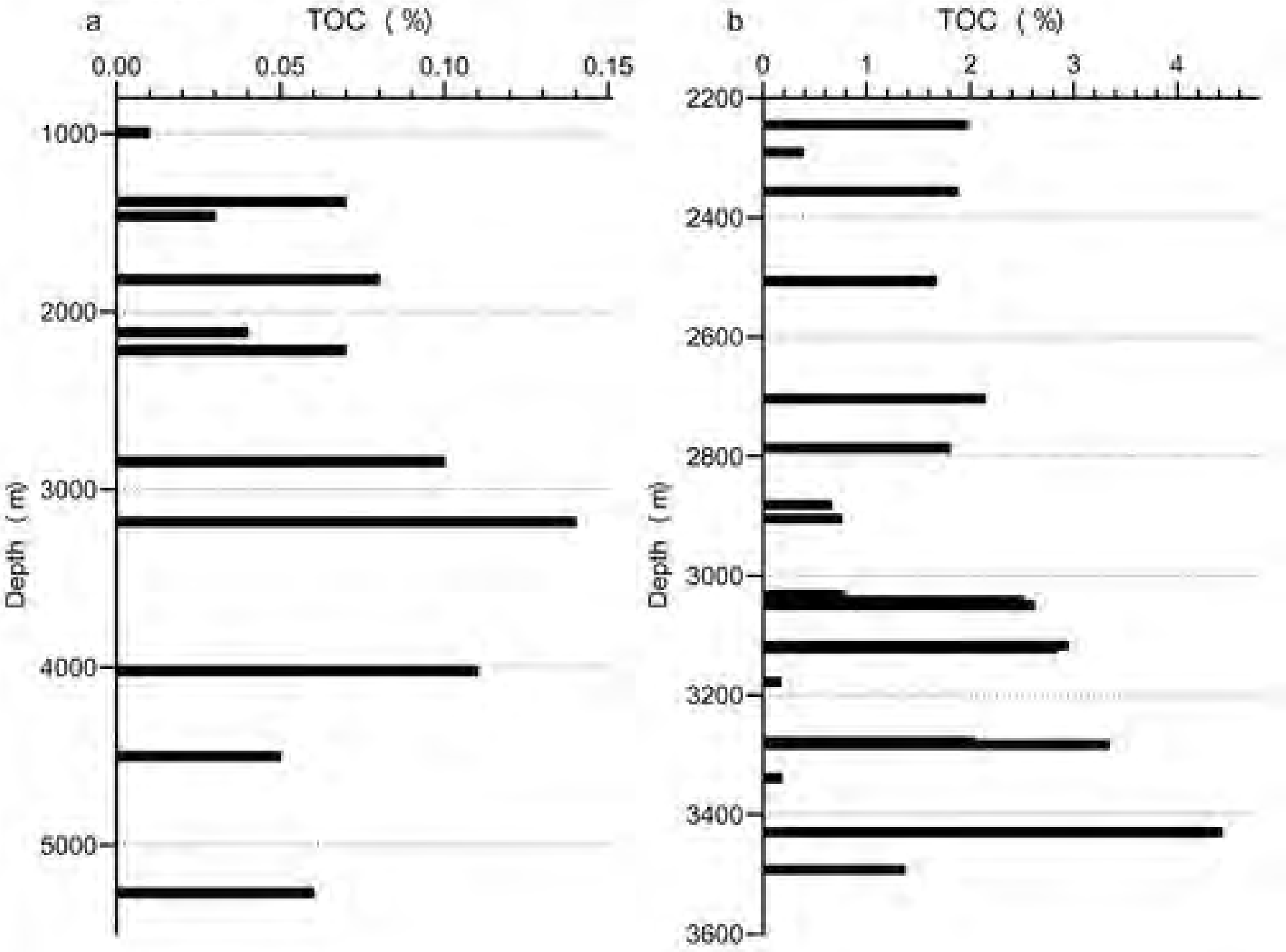
a
TOC (%)
0.00
0.05
0.10
0.15
1000
2000
3000
4000
5000
Depth (m)
b
TOC (%)
0
1
2
3
4
2200
2400
2600
2800
3000
3200
3400
3600
Depth (m)

Figure 6

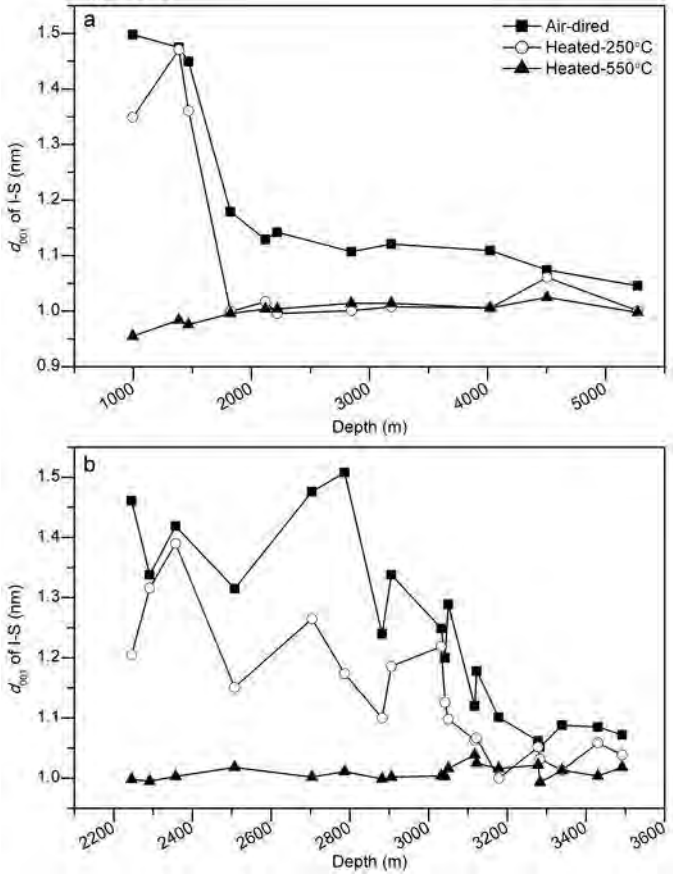
a
Air-dired
Heated-250°C
Heated-550°C
d_{001} of I-S (nm)
1.5
1.4
1.3
1.2
1.1
1.0
0.9
1000
2000
3000
4000
5000
Depth (m)
b
d_{001} of I-S (nm)
1.5
1.4
1.3
1.2
1.1
1.0
2200
2400
2600
2800
3000
3200
3400
3600
Depth (m)

Figure 7

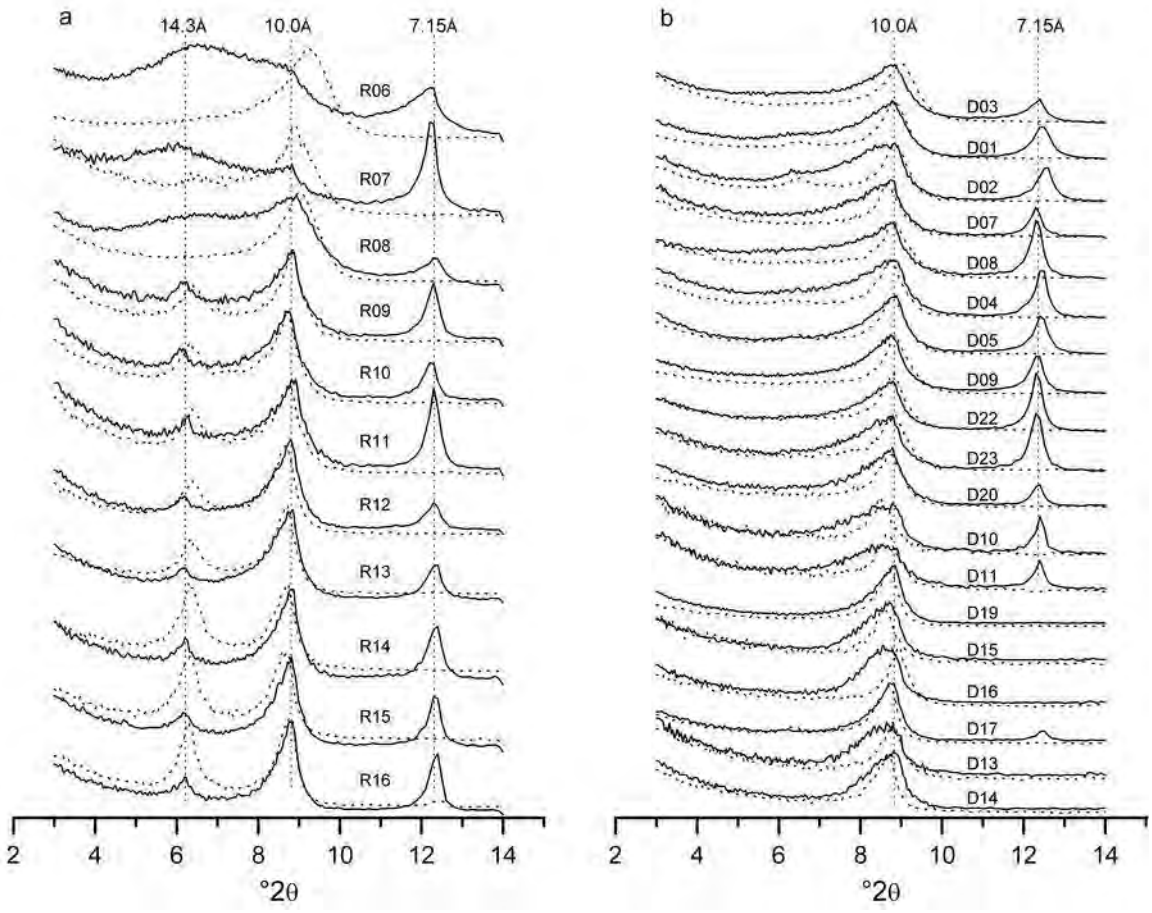
a
14.3Å
10.0Å
7.15Å
R06
R07
R08
R09
R10
R11
R12
R13
R14
R15
R16
2
4
6
8
10
12
14
°2θ
b
10.0Å
7.15Å
D03
D01
D02
D07
D08
D04
D05
D09
D22
D23
D20
D10
D11
D19
D15
D16
D17
D13
D14
2
4
6
8
10
12
14
°2θ

Figure 8

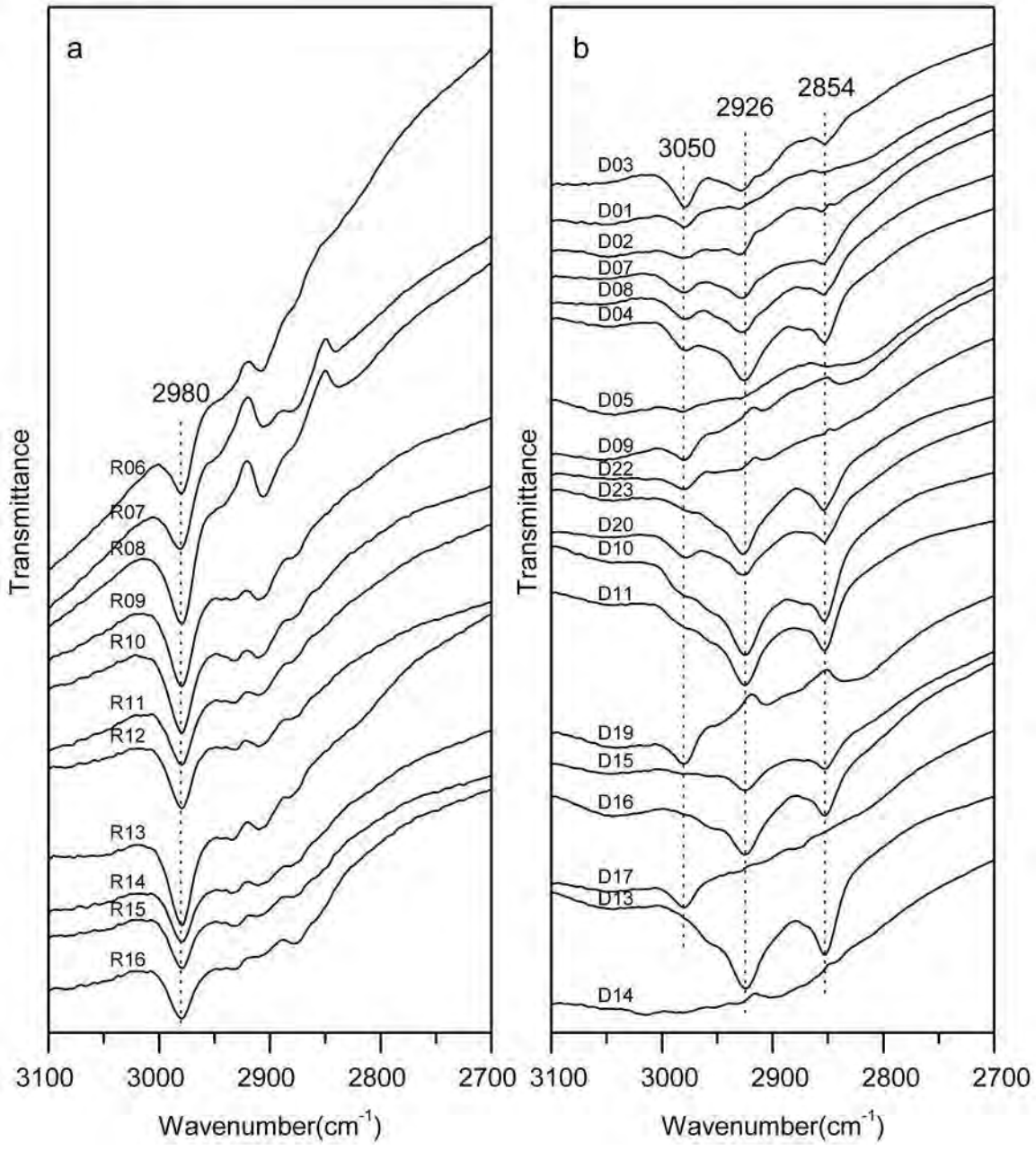
a
2980
R06
R07
R08
R09
R10
R11
R12
R13
R14
R15
R16
Transmittance
3100
3000
2900
2800
2700
Wavenumber(cm-1)
b
3050
2926
2854
D03
D01
D02
D07
D08
D04
D05
D09
D22
D23
D20
D10
D11
D19
D15
D16
D17
D13
D14
Transmittance
3100
3000
2900
2800
2700
Wavenumber(cm-1)

Figure 9

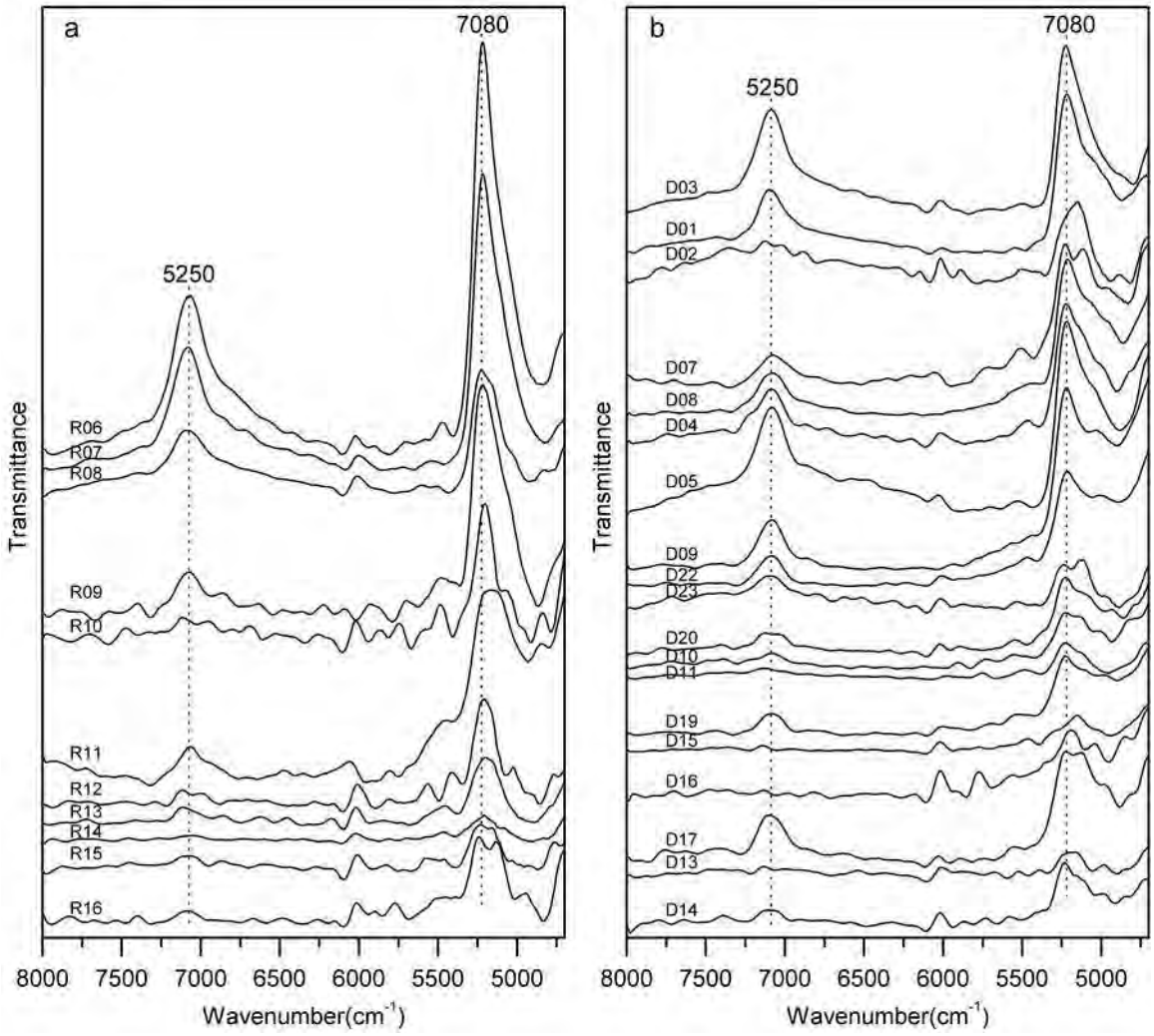
a
7080
5250
R06
R07
R08
R09
R10
R11
R12
R13
R14
R15
R16
Transmittance
8000 7500 7000 6500 6000 5500 5000
Wavenumber(cm-1)
b
7080
5250
D03
D01
D02
D07
D08
D04
D05
D09
D22
D23
D20
D10
D11
D19
D15
D16
D17
D13
D14
Transmittance
8000 7500 7000 6500 6000 5500 5000
Wavenumber(cm-1)

Figure 10

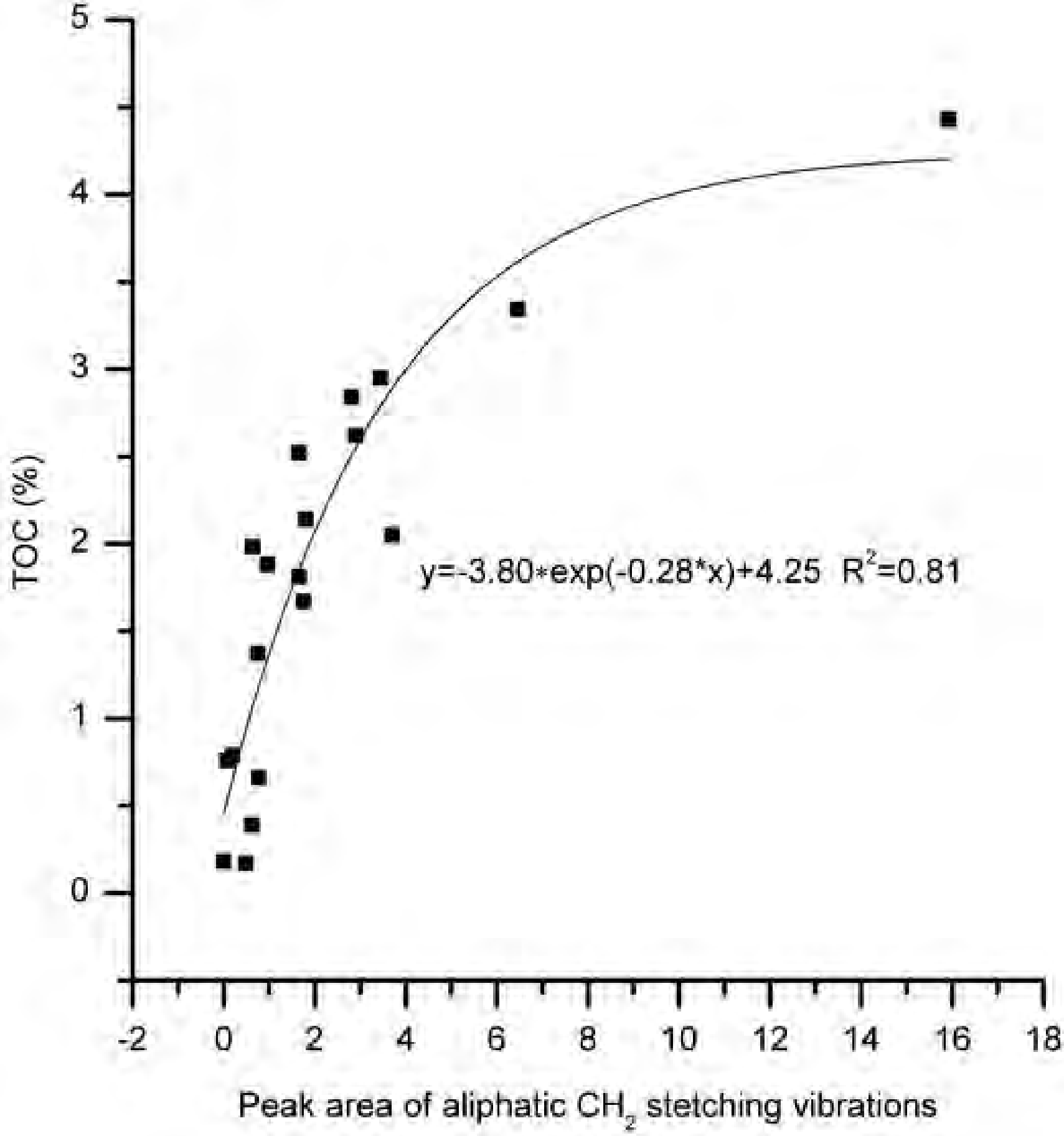
TOC (%)
0
1
2
3
4
5
-2
0
2
4
6
8
10
12
14
16
18
Peak area of aliphatic CH2 stetching vibrations
y=-3.80*exp(-0.28*x)+4.25 R2=0.81

Figure 11

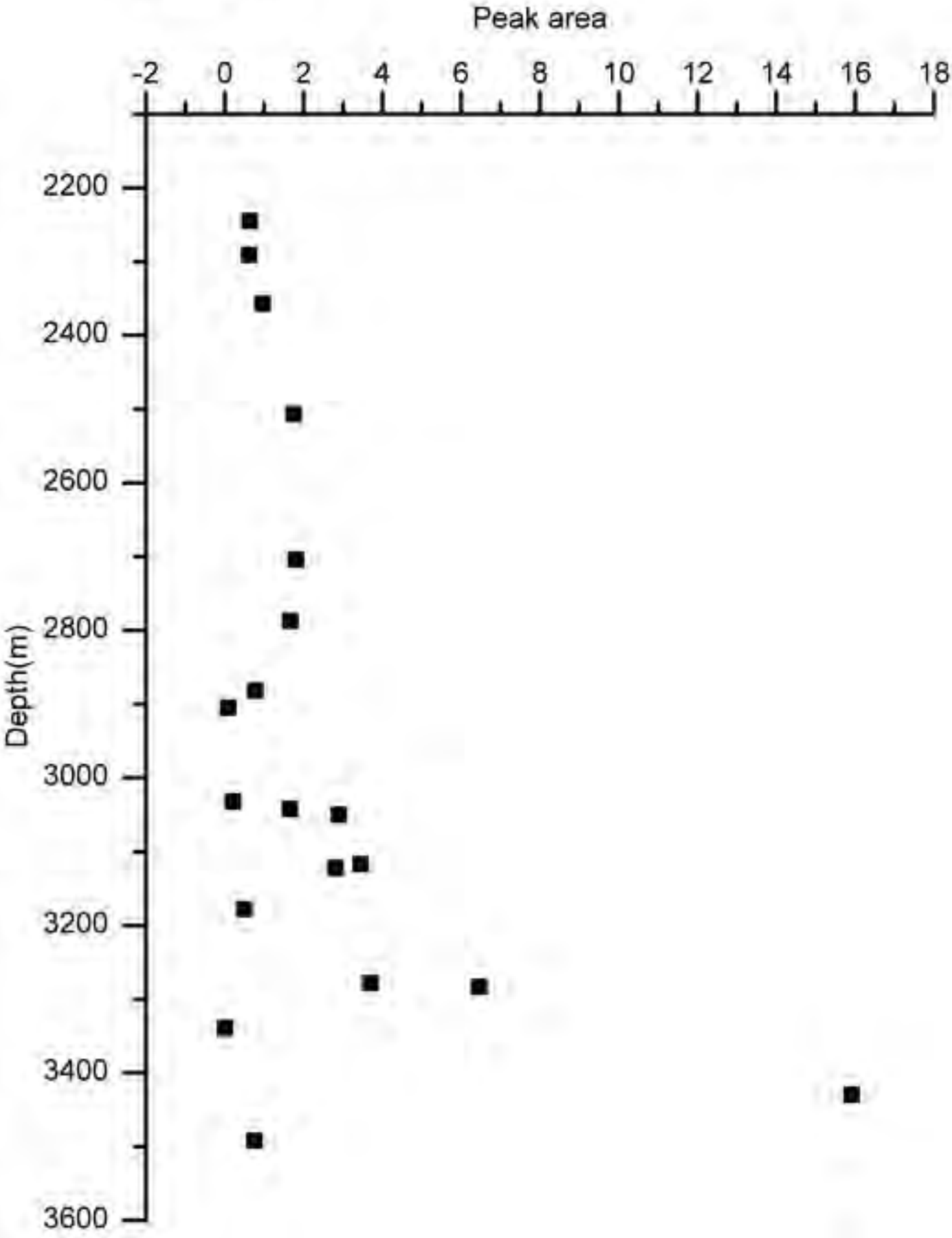
Peak area
-2
0
2
4
6
8
10
12
14
16
18
Depth(m)
2200
2400
2600
2800
3000
3200
3400
3600